A multi-spatiotemporal scale strategy to evaluate factors controlling pebble mobility and its interactions with bedforms in a lowland gravel-bed river

Thomas Dépret, Emmanuèle Gautier, Nathalie Thommeret, Hervé Piégay, Clément Virmoux, Janet Hooke, Delphine Grancher

A multi-spatiotemporal scale strategy to evaluate factors controlling pebble mobility and its interactions with bedforms in a lowland gravel-bed river

Thomas Dépret [a], Emmanuèle Gautier [a], Nathalie Thommeret [b], Hervé Piégay [c], Clément Virmoux [d], Janet Hooke [e], Delphine Grancher [d]

[a] Université Paris 1 Panthéon-Sorbonne, Laboratoire de Géographie Physique, CNRS UMR8591, 1 Place Aristide Briand, 92195 Meudon, France

[b] Laboratoire Geomatique et Foncier, CNAM-ESGT, 1 Boulevard Pythagore, 72000 Le Mans, France

[c] Université de Lyon, CNRS, UMR 5600 - Environnement-Ville-Société, Site ENS de Lyon, 15 Parvis René Descartes, Lyon 69342, France

[d] Laboratoire de Géographie Physique, CNRS UMR8591, 1 Place Aristide Briand, 92195 Meudon, France

[e] School of Environmental Sciences, University of Liverpool, Roxby Building, Liverpool L69 7ZT, UK

Highlights

- Very low bedload distances for full mobility floods at the event scale
- Weak trapping effect of bedload by bars at both event and decadal scales
- Bedload distances are lower than counterpart bedforms' distance at the event scale
- Bedload velocity varies depending on the year, bedform type or injection method
- Tracers' mixing was incomplete 10 years after their injection at the bed surface

Abstract

This paper aims to analyse how and what controls the spatiotemporal variability in bedload mobility in a low-energy gravel-bed meandering river, with a particular focus on the interactions between bedforms (bar-riffle-pool units) and bedload transport distance.

We first address the influence of pre-existing morphology, especially bars, upon the event transport distance, and examine to what extent the maintenance of bedforms requires the occurrence of hydrological events able to move the bedload over distances at least equivalent to the length of two successive identical geomorphic units. To do that, we tracked the displacement of PIT-tags particles 10 years after their injection and applied bedload formulas to reconstruct the event transport distance for a 32-year-long study period. Our results show that event bedload distances for the bed surface D_{50} could not exceed an active channel width, this one being roughly equivalent to 0.3 times the median distance between riffles and between pools. This has two main implications. First, the trapping effect by bars would be rare, or perhaps even absent, at the scale of competent events for most particles located at a distance greater than an active channel width from a bar. Second, because no event is able to transport bedload over distances at least equal to the length of one riffle-pool unit, the maintenance of bedforms and bars especially, would arise from successive minor changes.

Further, our data revealed important variability in the bedload velocity at a decadal scale according to the year of injection, the type of geomorphic unit of injection or the method of injection (i.e., cluster or cross-section). This highlights the long-term persistence effects in low-energy rivers upon velocity estimation from where, when and how tracers are injected.

Lastly, we inferred the long-term bedload velocity from the PIT-tags data and applied bedload formulas. Equal to 0.95–1.3 km century^{-1}, it is nevertheless considered an overestimate because the slowdown of tracers seeded at the bed surface, due to their progressive mixing in the active layer and their trapping in bars, was still on-going.

Keywords: Tracer dispersion; bedload path length; low-energy meanders; geomorphic units; active layer

1. Introduction

In coarse-bed rivers, the bedload is generally considered responsible for shaping much of the fluvial landscape (Andrews and Nankervis, 1995; Knighton, 1998; Leopold, 1992; Whiting et al., 1999). Identifying and characterising the modalities of bedload incipient motion, displacements, and deposits is therefore essential to improve our understanding of the conditions under which morphogenesis occurs. Bedload movements are generally viewed as stochastic processes (Bradley and Tucker, 2012; Einstein, 1937; Paintal, 1971; Roseberry et al., 2012), these mainly controlled by three groups of parameters: hydraulic and hydrological characteristics of the entrainment events, structural characteristics of the sediments, and finally, their textural characteristics (Gilet et al., 2020; Hassan et al., 1991; Hassan and Church, 1992; Vázquez-Tarrío and Batalla, 2019). Yet the distance travelled by the bedload during a competent event does not always depend on stochastic processes alone (Pyrce and Ashmore, 2003a, 2003b). In addition to being influenced by the recent flow history and/or sediment supply (e.g. Buffington and Montgomery, 1999; Church et al., 1998; Dietrich et al., 1989; Downs and Soar, 2021; Hassan and Church, 2001; Hassan et al., 2020; Haynes and Pender, 2007; Konrad et al., 2002; Lisle et al., 1993, 2000; Mao, 2012; Masteller et al., 2019; May and Prior, 2014; Monteith and Pender, 2005; Nelson et al., 2009; Ockelford and Haynes, 2013; Paphitis and Collins, 2005; Reid et al., 1985), both bed mobility and bedload distance could also be governed and constrained by a bed's morphology; i.e., its organization in well-structured geomorphic units, or bedforms. Accordingly, many researchers have hypothesized that event transport distances scale with certain metrics that characterize bed morphology. These are considered equivalent to the distance between an erosion zone and the closest downstream deposit zone (e.g., Ashmore and Church, 1998; Carson and Griffith, 1989; Eaton and Lapointe, 2001; Gaeuman et al., 2003; Lane et al., 1995; Neill, 1971, 1987). This assumption has been extensively explored using various approaches that aim to estimate the transported volumes by applying the inverse method (Ashmore and Church, 1998; Church, 2006). Furthermore, the influence of bed morphology on travel distance, real or presumed, is more or less explicit in numerous studies (e.g., Beechie 2001; Hassan and Church, 1992; Hassan et al., 1991; Hassan and Bradley, 2017; Kasprak et al., 2015; Kondolf and Matthews, 1986; Lamarre and Roy, 2008; McDowell and Hassan, 2020; McDowell et al., 2021;

McEwan, 2001; McQueen et al., 2021; Papangelakis and Hassan, 2016; Pyrce and Ashmore, 2003a, 2003b, 2005; Schmidt and Gintz, 1995; Sear, 1996; Vázquez-Tarrío et al., 2019).

According to Pyrce and Ashmore (2003a, 2003b), the distribution of transport distances can be categorised into four types, as distinguished by the intensity and duration of bedload-mobilizing events. The first two types (types A and B in Pyrce and Ashmore, 2003a) correspond to non-morphogenic events. In both, the vast majority of particles are not mobilized or only transported over very short distances; bedload displacements are hardly, or not at all, controlled by the bedforms, and; shear stresses are slightly higher than the critical stress value and transport is partial. The last two types (types C and D) correspond to morphogenic events. In both, transport distances are less dependent on the duration and magnitude of floods, and instead increasingly influenced by bed morphology; shear stresses exceed greatly the critical stress value and the bed eventually becomes fully mobile. Thus, in the case of competent events that are sufficiently long and intense, the modal displacement distance is only partially determined by flood characteristics (duration or intensity). Most of the material is then deposited on bars. For riffle-pool systems, transport distances are equivalent to the distance between a pool and the downstream bar; i.e., the distance separating two successive identical geomorphological units (Pyrce and Ashmore, 2003a, 2003b, 2005). Finally, during the longest and/or most intense floods, transport distances are mainly controlled by the characteristics of hydrological events (Pyrce and Ashmore, 2003a, 2003b, 2005; Reid et al., 2007). These events are potentially able to either remodel or destroy the original morphology of the bed, by removing or remodelling the bars—thereby in effect limiting their influence on transport distances—or remobilizing particles after their initial deposition on bars. Although based on many field studies and flume experiments, this conceptual model needs to texted against a larger range of rivers and conditions to further assess its validity (Pyrce and Ashmore, 2003a). Alternatively, Pyrce and Ashmore (2003a, 2005) also argued that the development and maintenance of these bedforms, especially bars, requires the occurrence of hydrological episodes able to transport the bedload over a distance similar to that between two successive bars, equivalent to the length of a single riffle-pool unit. The existence of such morphology is hypothesized to result from the "net outcome of individual particle displacements from discrete erosion loci" (Pyrce and Ashmore, 2003a). However, that would imply that bedforms are shaped by hydrological events with sufficient power for full mobility to occur, which

raises the question of whether such morphogenesis processes actually occur in low-energy gravel-bed rivers flowing in a temperate environment, notably those having coarse bedload particles. Indeed, in the case of most gravel-bed rivers, and more so for low-energy rivers, the highest shear stresses attained are often only slightly greater than the critical shear stress. According to earlier work by Parker et al. (1982), the ratio between the Shields stress and the critical Shields stress in most gravel-bed rivers almost never exceeds a value of 2–3. Nevertheless, full mobility may only occur when this ratio is > 2 (Wilcock and McArdell, 1993; Church and Hassan, 2002; Recking, 2010). Furthermore, in temperate environments, the difference in energy between frequent and rare flood events is generally low (Baker, 1977; Kochel, 1988; Lewin, 1989; Magilligan, 1992). These diverse aspects imply that in such systems, at least for some, full mobility would be rarely attained (Church, 2006; Haschenburger, 2017; Haschenburger and Wilcock, 2003). Yet, paradoxically, many of these rivers have a clearly discernible riffle-pool structure.

Here, we mainly examine the two sides of the conceptual model of Pyrce and Ashmore (2003a, 2003b), by conducting an in-depth case study of a low-energy gravel-bed river. We focus on the interactions between transport distance and morphogenesis in a meandering reach of the Cher River in France across different temporal scales. Because of this river's low energy, we formulated two principal hypotheses, both related to the assumed low event transport distances. First, only those particles located at very close distances to bars could become trapped in them. Second, bedforms would be maintained without the need of transport events whose distance is at least equal to the length scale of the riffle-pool units.

To that end, using PIT tags, annual and decadal bedload transport distances were measured between 2010 and 2020 along a meander bend. The distance travelled by the bed surface D_{50} at either time scale was compared to that estimated according to recent bedload formulas. The ones best able to predict the tagged particle distance at both yearly and decadal scales were then used to determine the event transport distance for the entire discharge record period (i.e., 1988–2020) and then infer the centennial bedload distance. Next, the distances obtained at the event and decadal scales were compared to the distance separating successive identical geomorphic units. Finally, the tracers' 10 years of data was used to investigate (1) the variability in bed mobility and velocity according to year, type of geomorphic unit, and method of tracers' injection, and; (2) the way in which tracers were mixed within

138 the active layer. A key assumption being that the river's low energy confers a long-term persistence of
139 the effect on bedload velocity estimation arising from where, when, and how tracers are seeded.
140
141 **2. Study site**
142 After leaving its source at 713 m a.s.l., the Cher River mainly flows through gorges across steep slopes
143 or in deep valley with a very narrow floodplain (upstream Cher in Figure 1). The 63-km-long upstream
144 reach of the river is located at the northwest end of the low-elevation mountainous Massif Central
145 (France), which mainly consists of crystalline and metamorphic rocks (Larue, 1981, 2011). Then, the
146 alluvial plain begins (Alluvial Cher in Figure 1), and the river becomes single thread with a meandering
147 pattern that developed over the last millennia (Vayssière et al., 2020). After first occupying the Tertiary
148 graben of Montluçon, running 45 km to the confluence with the Aumance River (Larue, 1981, 2011;
149 Simon-Coinçon et al., 2000), the river then crosses the sedimentary domain of the Parisian Basin, where
150 it joins the Loire River at a 38 m a.s.l.
151 At the reference gauging station for our study site (Figure 1), the mean annual discharge is 14.8
152 $m^3 s^{-1}$. The rainfall regime is typical of lowland rivers on the western facades of mid-latitude regions.
153 The minimum and maximum monthly discharges occur respectively in August and February. The
154 hydrological regime, particularly the low-flow regime, is partly affected by the Rochebut Dam, it located
155 45 km upstream of the study reach, whose construction was completed in 1909 (Figure 1). Initially built
156 exclusively for electricity production, the dam has since been relied on to provide low-water support for
157 several decades now.
158 The study reach spans more than 700 m along a meander bend located in the Tertriary graben
159 of Montluçon (Figure 1). Its bedrock is composed of Eocene and Oligocene sand and clay on the left
160 side of the valley, and of Triassic sand more or less clayey on its right side (Turland et al., 1989a). The
161 alluvial infilling is schematically organized into two or three main stratigraphic levels. The base of the
162 infilling consists of sand, gravel, and pebble while its upper part consists of overflow deposits of clay,
163 silt, and sand (Dépret, 2014; Turland et al., 1989b); between these two levels, a predominantly sandy
164 layer is often interspersed. Because of this composite structure and the coarse nature of its material, the
165 banks are highly erodible (Dépret et al., 2015, 2017). But due to the presence of ancient fluvial

engineering works, especially those protecting the bank, the historical mobility of the reach is low (Dépret et al., 2015, 2017).

The active channel width is 32 m, the low-flow bed slope is 0.001133 m m^{-1}, and the bankfull discharge is 85 m^3 s^{-1} at the reference gauging station, this one located at Montluçon (Figure 1). With a surface D_{50} and D_{84} of 28 and 48 mm, respectively, and a bankfull specific stream power of 30 W m^{-2} (computed from the active channel width), it is a low-energy river with a coarse gravel bed (Dépret, 2014; Dépret et al., 2015). In the study bend, the armour ratio for the D_{50} and the D_{84}, as determined in two riffles, is equal to 2.7–3.2 and 1.3–1.5, respectively (Dépret, 2014). These relatively low values are consistent with the quite high frequency of mobilization of D_{50} (34 days y^{-1} for a critical discharge of 40 m^3 s^{-1}) and the fact that the whole grain-size spectrum can be mobilized for discharge below the bankfull (Dépret et al., 2017). These features strongly suggest a relatively weak sedimentary deficit, and thus, at worst, a slight reduction in bed mobility because of the fluvial engineering works' presence or due to the Rochebut Dam. An absence of the latter's influence is explained by the very lightly modified hydrological regime for a discharge higher than the critical discharge, and by the fact that the total interruption of the bedload continuity it has induced has not yet affected the study site. Comparing the natural reconstructed daily discharge at the dam's outlet (powered discharge + variation of water level in the reservoir + discharge above the crest of the dam; data provided by Electricité de France) with the actual daily discharge outflowing from it (powered discharge + discharge above the crest of the dam; data from https://hydro.eaufrance.fr/) shows that the annual number of days exceeding the critical discharge is 1.2-times higher for the former than the latter. Concerning the peak of competent events, the actual discharge values are just slightly lower than the natural reconstructed ones ($ActualQ = 1.04 \times NaturalQ - 6.7$, $R^2 = 0.95$). Lastly, the distance between the Rochebut Dam and the study site is more than 10-fold the distance travelled by bedload since the dam's completion. Hence, the bedload deficit due to the dam could not have yet reached the study site.

The bedforms are organized into well-developed riffles and pools, some of them forced due to the presence of the fluvial engineering works in the bed (Buffington et al., 2002; MacVicar et Roy, 2011; Thompson et Wohl, 2009). Therefore, the pools P1 and P2 can be separated in two sub-pools (named A and B) according to the presence of a structure similar to a groyne (Figure 2). P3 is also

separated into two sub-pools (A and B) according to the presence of remnants of bank protections in the bed. P1B, P2B, and P3B are thus at least partly forced. Furthermore, the pool P3A as well as the riffle R3 are also probably forced given the presence of two crosswise, parallel alignments of piles on the right half of the bed, these exhumed due to bank erosion over recent decades (Figure 2). Furthermore, some bars are evident. The two main ones are situated at the upstream and downstream boundaries of the bend equipped with tracers (Figure 2). The downstream one (B4) is located along the study reach's main section, where lateral mobility has occurred in the last decades. For this reason, it has grown laterally during the study period, whereas the other bars have remained more stable.

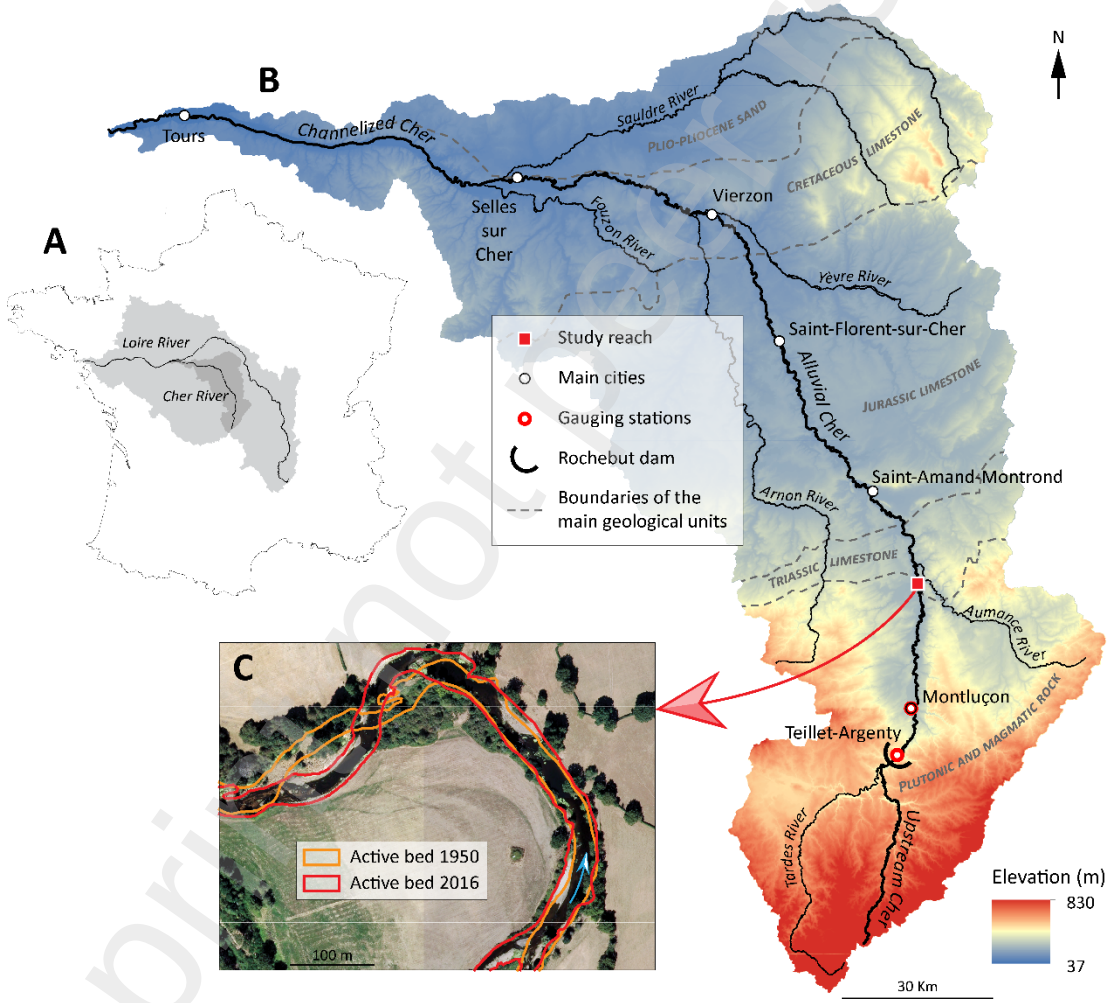

Figure 1 – Study site localization. A: The Cher River watershed within French territory. B: The study reach in the Cher River watershed. C: Zoom on the study reach.

3. Material and methods

3.1 PIT-tags and bedload velocity from 2010 to 2020

Bedload velocity was estimated at an annual and decadal scale on a meander bend by tracking particles equipped with passive transponders (Texas Instruments RFID chips, length: 12–23 mm, emission frequency: 134.2 kHz). A total of 1503 tagged particles were injected in 2010, 2011, and 2012 into the different geomorphological units of the bend (i.e., riffles, pools, bars) as well as into the two active banks and at their toe (Figure 2). Previously, the geomorphic units were identified visually and delineated with an RTK-DGPS: we distinguished riffles, pools, bars and also the main glides or runs. Portions of some pools were also apparently forced (see section 2). Two injection strategies were used in tandem, whereby tracers were introduced individually or in clusters. Individual tracers were injected in 2010 and 2012 at 50-cm intervals along cross-sections located at the head of riffles. The total number of particles per cross-section ranged from 32 to 53. Clusters were injected in 2010 and 2011, with 40 particles per cluster. In 2010, they were deposited in the centre of each of riffle and likewise in two of the pools (P1A, P2B), and also at the head of the main migrating bar (B4) and in the banks as well as at their toe (Figure 2). An identical strategy was implemented for the 2011 clusters, this time with all the pools and the upstream run equipped with them (Figure 2). Clusters at the bank toe were positioned midway between the upstream and downstream limits of the active banks. Clusters in banks were positioned at three longitudinal locations: at the vertical of the clusters located at bank toe, and midway between that point and the upstream or downstream limit of the active banks. Two clusters per vertical were placed in the upstream bank (at mid-height and between that and the top of the bank), one in the downstream bank (at mid-height). Except for the deepest pools (i.e., P1A, P1B, P2B, cf. Figure 2), all the tagged particles were inserted into the pre-existing sedimentary structure, in order to avoid artificial overexposure to the flows. For riffles, the particle size of tagged particles corresponds to the channel's surface particle size (from 22.6 mm), as determined in 2010 by sampling 400 particles according to the Wolman's methodology (1954). For the other geomorphic units, the tracers' particle size distribution was the same as that for the riffle located immediately upstream. Each half-phi size-class was tagged between 22.6 and 90.5 mm. For banks, only the 22.3–32 mm and the 32–45 mm classes were equipped. Three detection surveys were carried out in summer at low flow, one each in 2011, 2012, and 2020

(detection system built by CIPAM). The detection front was located 180 m from the downstream-injection cluster in 2011 and 2012 (for a maximum and a 99% percentile of particle distances of 232 m and 117 m, respectively, for the 2010–2012 period). In 2020, the detection front was located 1200 m from the downstream-injection cluster (maximum and 99% percentile of particle distances of 1200 m and 720 m, respectively from 2010/2011/2012 to 2020). The position of each particle was surveyed manually with an RTK-DGPS in the wadeable portions of the bed. For the rest of the bed, particles' detection required the use of a boat. In 2011 and 2012, the boat was attached to ropes stretched across the bed; in 2020, their detection was performed with an electric motor boat, the RFID reader and the RTK-DGPS being connected to a laptop, with the position and identification of every tracer automatically recorded (ArpenGIS software).

For particles individually injected along the cross-sections, the critical distance of mobilization was set to 40 cm, which corresponds roughly to the maximum detection range of the antenna (Arnaud et al., 2015; Chapuis et al., 2014). For clusters, the determination of this distance took into account the uncertainty related to the initial position of each particle, as well as any uncertainty concerning the location of the particles at the time of their detection. The exact initial position of each particle could not be precisely known because we only had the coordinates for the centre of each cluster. Therefore, the value of the first type of uncertainty is equal to the radius of clusters (40 cm in 2010, and 30 cm in 2011). The second type of uncertainty is linked to the maximum detection range (20 cm) of the small antenna used to detect tracers located near the clusters. For most clusters, the total uncertainty, and hence the critical distance of mobilization, was 60 cm (40 cm + 20 cm) for the 2010 particles and 50 cm (30 cm + 20 cm) for the 2011 particles. For some clusters located in pools, the critical distance was longer because of greater uncertainty associated with the initial position and/or location of the particles (2 m for M1A, P1B, and P2B; 0.8 m for P3A, P3B, and P4).

3.2 Characterization of bedload mobility, velocity, and trajectory at a decadal scale

For all particles, and likewise for each half-phi grain-size class, we first calculated the recovery rate, the mobilization rate, as well as the mean and median distances travelled by the detected particles (mobilized and non-mobilized). We also investigated how these parameters varied by date, by unit, and

by method of injection (cross-sections or clusters). To enable such comparisons, we distinguished those particles injected in clusters into the same units in 2010 and 2011 (i.e., five riffles and two pools), particles injected in clusters into riffles only in 2010 and 2011 (fives riffles), particles injected along cross-sections in 2010 and 2012 (four riffles), particles injected in clusters into pools in 2010 and 2011 (two pools in 2010, seven in 2011).

Next, we examined the distances and trajectories of particles, to determine how they interacted with the river's size and its geomorphic units, especially bars. To do that, we first calculated the percentage of particles (mobilized and non-mobilized) that were deposited in their unit of injection or in the downstream one. Then we compared the 10-year distance travelled by particles (= 10 times the annual velocity of 2010 or 2011 or 2012 particles between their year of injection and 2020) to the median distance between successive riffles and between successive pools (110 m); the percentage of travelled distances lower than the median distance between units was determined. We also characterized the influence of the only laterally developing and migrating bar (B4) upon the trapping efficiency of particles at a decadal scale. For each geomorphic unit of tag injection upstream of the bar (all dates, clusters, and cross-sections taken together), we looked at the percentage of all particles and those of 22.3–32 mm in size that got trapped in the bar and examined how it varied with distance to the bar. Finally, we focused on particles injected in banks and at the bank toe, to better understand how particles eroded from the banks are redistributed in the active channel.

3.3 Distribution of particle velocities at a decadal scale

The shape of the velocity distribution and of its tail was examined, to gain insight into the dispersion of tracers occurs and because it has major implications for modelling advection-diffusion processes (Haschenburger, 2013; Hassan et al., 2013; Hassan and Bradley, 2017). First, we determined how well (or not) various probability distributions widely tested in the literature fitted with the annual velocity distribution (for all generations of tagged particles taken together and for each generation considered individually, for all particle sizes and only those 22.3–32 mm in size). Following the probability distributions tested by Haschenburger (2013) and Papangelakis and Hassan (2016), and according to the shapes of the annual velocity distributions, we tested four types of probability distributions using the

'fitdistrplus' package in R (Delignette-Muller and Dutang, 2015): the exponential, gamma, Pareto, and Weibull. Akaike's Information Criterion (AIC) was used as goodness-of-fit criterion between the probability distributions (Delignette-Muller and Dutang, 2015). Second, we focused on the behaviour of the distributions' tail. To do this, we implemented two approaches developed by Hassan et al. (2013). In one, a power law is fitted to the tail of the exceedance probability distribution of tracer velocities, using ordinary least-squares regression, and the fitted power value examined. Heavy and thin tails respectively correspond to a log–log slope of the exceedance tail of $\alpha < 2$ and $\alpha > 2$. The other approach relies on Hill's estimators (Hill, 1975), a ranking method based on the conditional maximum likelihood estimator for the power and slope in the Pareto distribution $P(X > x) = Cx^{-\alpha}$ fitted to the tail of sample data:

$$\alpha_H = r\left[\sum_{i=1}^{r}(ln\, X_i - ln\, X_{(r+1)})\right]^{-1};\ C_H = \frac{r}{n}(X_{(r+1)})^{\alpha_H}$$

where α_H and C_H are estimators for power and slope, respectively; X_i are the order statistics such that $X_1 \geq X_2 \geq \ldots X_n$; the r is the rank of the smallest data point in the tail of the distribution. When $\alpha_H < 2$, the distribution is considered to be heavy-tailed.

3.4 Estimation of bedload distance at the event-based and century scales

To estimate the bedload velocity at the event-based scale, we tested the most recent formulas published in the literature (eq. 4 in Gilet et al., 2020; eq. 13, 14 for all rivers, eq. 14 for riffle-pool rivers, and eq. 15 for riffle-pool rivers in Vázquez-Tarrío and Batalla, 2019; eq. in figure 2 for riffle-pool rivers with width/depth bankfull ratio > 10 in Vázquez-Tarrío et al., 2019; eq. for riffle-pool rivers in figure 4 in Vázquez-Tarrío et al., 2019; eq. for all rivers except for the unconstrained step-pool rivers in Figure 9 in Vázquez-Tarrío et al., 2019). Derived from field data, these formulas relate the event bedload velocity or distance to different controlling parameters, such as flood magnitude and duration, grain-size of the bed, and the width and slope of the river, among others. Here we selected the ones providing the closest estimate of empirical distances travelled by the PIT-tags in the periods 2010–2011, 2011–2012, 2010–2020, 2011–2020, and 2012–2020. Here we postulated that if the formulas are robust for reconstructing the cumulative event bedload distance at yearly and decadal scales, they should be reliable for estimating

the event bedload distances. On this basis, the chosen formulas were applied to each competent event that occurred for the entire daily discharge record period (i.e., 1988–2020 at the Montluçon reference gauging station). The critical discharge for incipient motion was first estimated from presence–absence PIT-tags surveyed at different discharge values between 2010 and 2012 along the cross-sections located at riffle heads (Dépret et al., 2015, 2017) (R1, R3, R4, R5, cf. Figure 2). It was also estimated from six 20-mm sensitive 'Benson-type' seismic impact plate sensors (Downs et al., 2016), these equally spaced along a cross-section located at the riffle head on the bend downstream of the PIT-tag bend, which recorded data during the 2018–2019 high-flow period. Both approaches provided an estimation of the critical discharge equal to 40 $m^3 s^{-1}$ at the Montluçon reference gauging station. In addition to the critical discharge, to apply the formulas three other parameters must be known: the surface grain-size, the bed slope, and the active channel width. Surface grain-size was determined from low-flow photographs in 2018 of coarse grain-size patches of each bar. The photographs were taken vertically with the scene hidden from direct solar radiation, at a high enough resolution to distinguish particles as small as coarse sand. Using GIS (ArcGIS 10.6), we measured the apparent b-axis of 100 particles located at intersections of a regular grid on the photo, whose spacing was higher than the maximum longest axis (a-axis). The D_{50} and D_{84} used in formulas corresponded to the interpolated D_{50} and D_{84} of bars (28–48 mm), being very close to the values obtained from the Wolman samples on riffles in 2010 (25–44 mm). The slope was surveyed at low flow with a RTK-DGPS in 2020. The active channel width was reconstructed from a 2016 aerial orthophotograph (provided by the IGN: Institut Géographique National) analysed in GIS; after the active channel's digitization, its surface area was divided by the length of the study reach to obtain the average width.

3.5 Interactions between bedforms and bedload distance at the event scale

For a channel-forming discharge, namely for conditions of full mobility, and in the presence of well-developed riffle-pool morphology, the modal event bedload velocity should be controlled by the distance separating a pool to the bar located immediately downstream, the latter trapping most of the particles (Pyrce and Ashmore, 2003a, 2003b). Conversely, this implies that for such a discharge, particles should be able to displace to a distance at least equal to that separating two successive identical

geomorphic units. To test where that applies to the Cher River, we compared the event distances to the median distance between successive riffles and between successive pools (sub-pools considered here as individual units). The conditions for full mobility are theoretically reached when the grain shear stress exceeds twice its critical value (Wilcock and McArdell, 1993; Church and Hassan, 2002; Recking, 2010). To determine if events with full mobility had occurred from 1988 to 2020, the shear stress value for which full mobility begins was derived, using two slightly different methods. In the first one, we followed Recking et al.'s (2016) formula for riffle-pool rivers, which estimates the Shields stress corresponding to the transition from partial to full mobility:

$$\tau_m^* = (5S + 0.06)\left(\frac{D_{84}}{D_{50}}\right)^{4.4}$$

where S is the bed slope (in m m^{-1}); D_{50} and D_{84} respectively are the median and 84th percentile of the surface grain-size distribution (in m).

In the second method, we calculated the Shields stress value for the critical discharge, this corresponding to incipient partial transport, multiply it by two to determine the Shields stress for full mobility. The critical Shields stress was computed for the D_{84}, since it allows approaching the grain stress without any bias (Recking et al., 2016), as follows:

$$\tau_c^* = \frac{\tau}{(\rho_s - \rho)gD_{84}}$$

where ρ_s is the density of sediment, ρ is the water density, and τ is the critical bed shear hear stress (in N m^{-2}), the last obtained this way:

$$\tau = \rho g S d$$

where g is gravity acceleration (9.81 m s^{-1}); d is the average flow depth (in m), computed as follows from the approximation of Rickenmann and Recking (2011) proposed by Recking et al. (2016):

$$d = 0.015 D_{84} \frac{q^{*2p}}{p^{2.5}}$$

where $p = 0.24$ if $q^* < 100$ or 0.31 otherwise (which is the case of our study reach), and $q^* = q/w\sqrt{gSD_{84}^3}$, for which q is the water discharge (in $m^3\ s^{-1}$).

For overbank flows (i.e., those > 85 $m^3\ s^{-1}$), the discharge q used is the one for the prism over the channel. The bed mobility is controlled by this discharge value rather than by the total discharge. Following Dépret et al. (2015), we used the results of a hydraulic modelling done in 1998 (Direction Départementale de l'Allier, 1998) for seven flood discharge values along a cross-section located at riffle R1. From it, a power law was obtained to predict the discharge over the channel as a function of total overbank discharge:

$$q = 9.872 Qtot^{0.487}$$

where $Qtot$ denotes the total overbank discharge (in $m^3\ s^{-1}$).

Then, according to both methods, we determined the discharge corresponding to the Shields stress for full mobility. Each value was compared to the peak discharge of each competent event, to identify those events in which the theoretically full mobility had occurred. Finally, for each event, we compared the mean bedload distance to the median distance between riffles and between pools (110 m).

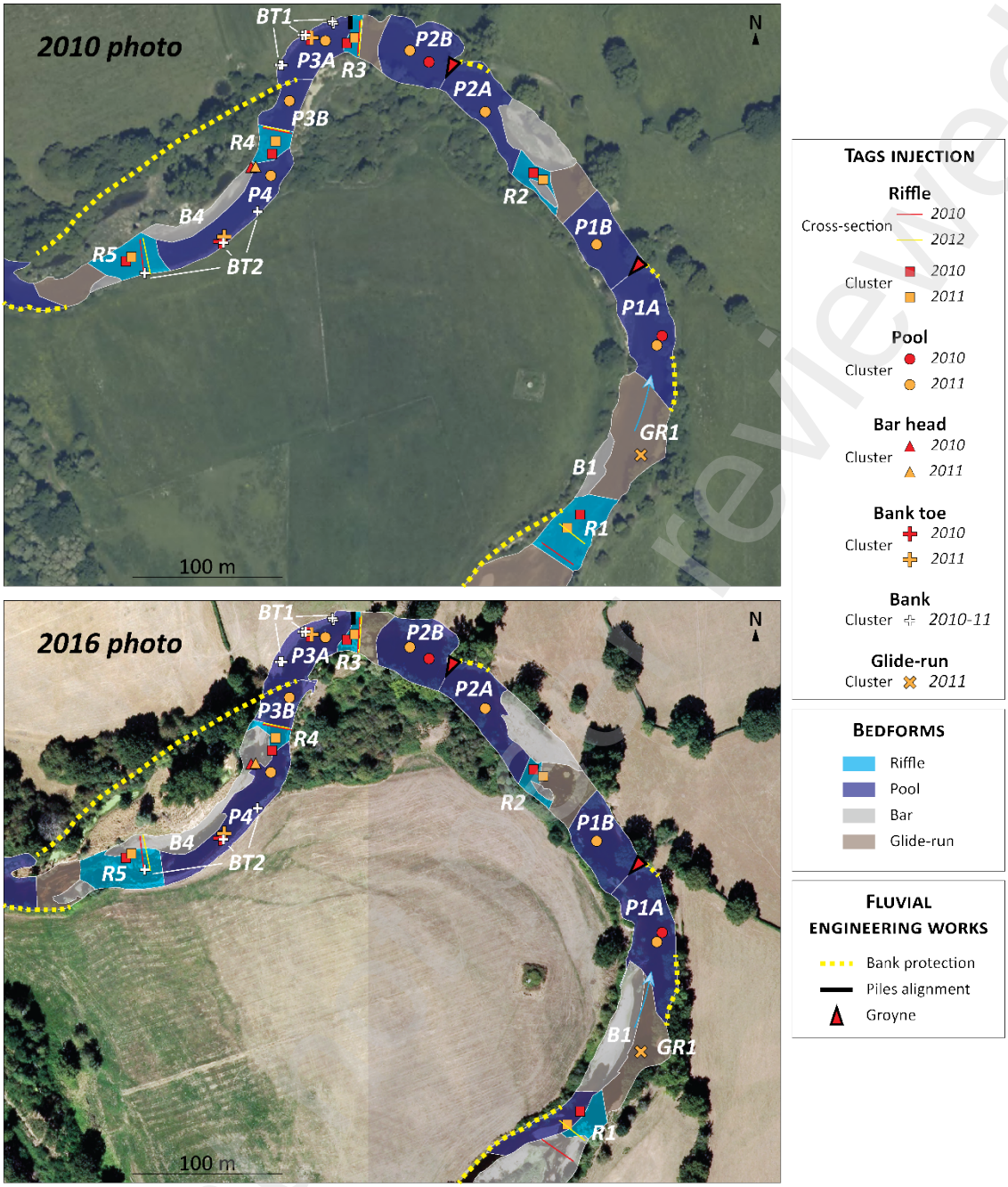

Figure 2 – Localization of the PIT-tags' injection and of the fluvial engineering works in the study reach; delineation of the main geomorphic units in 2010 and 2020.

4. Results

4.1 2010-2020 recovery rate and mobilization rate

The recovery rate for all particles injected into the bed across all dates is 59% irrespective of injection year (Figure 3). Moreover, it increased with particle size: being 45% (40%– 49% according to the injection year), 59% (51%–62%), 73% (70%–75%, 78% (75%–82%) respectively for the particle size-

404 classes of 22.3–32 mm, 32–45 mm, 45–64 mm, and 64–90.5 mm (Figure 3). For particles injected into
405 banks, the overall recovery rate was 53% (52% for injected particles in 2010, 55% for those in 2011).
406 Considering individual injection points (cluster or cross-section), the recovery rates varied from 32% to
407 100% (Figure 4A).

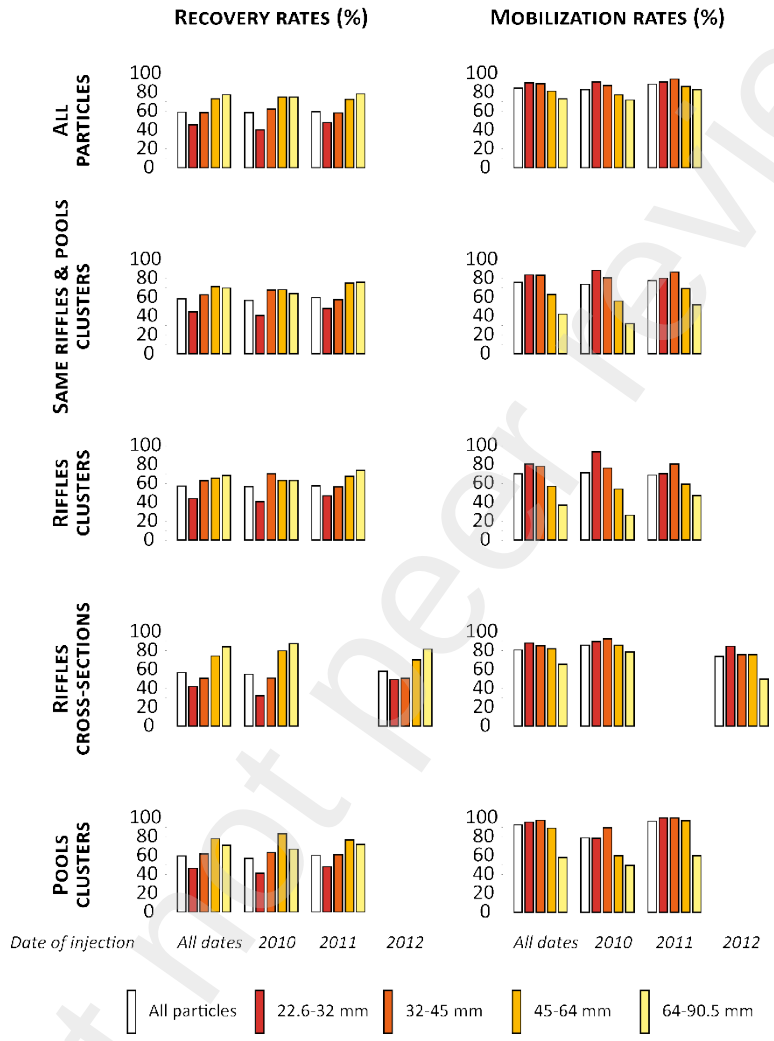

408

409 Figure 3 – Recovery rates and mobilization rates of tracers from 2010/2011/2012 to 2020.

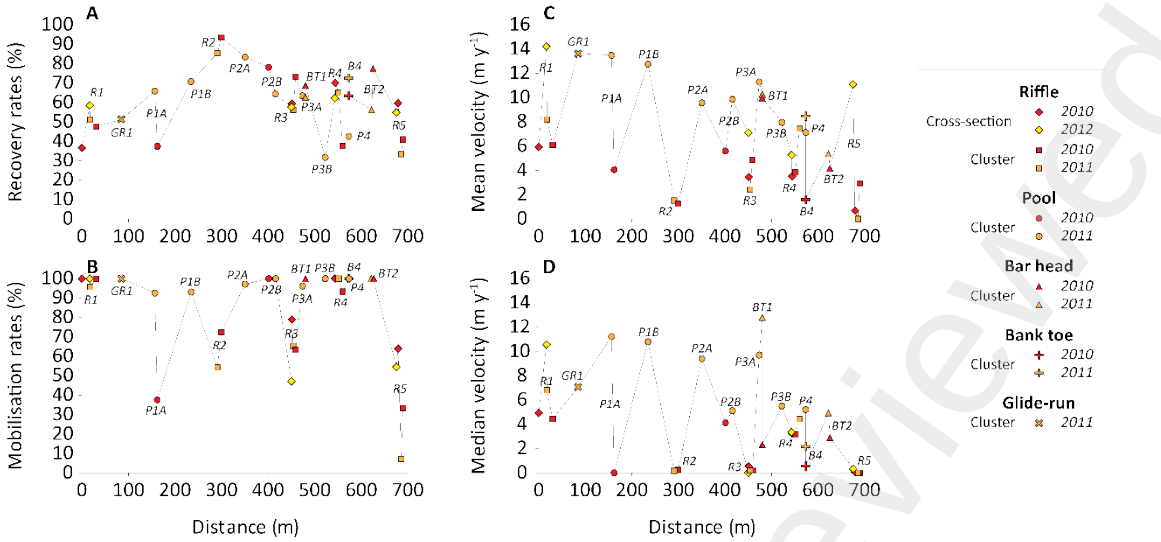

Figure 4 – Longitudinal pattern of recovery rates (A), mobilisation rates (B), mean velocity (C), and median velocity (D) for all particle size-classes taken together.

The mobilization rate for all particles injected into the bed for all dates is 84% (83% for 2010 particles, 89% for 2011 particles, and 73% for 2012 particles). It decreased slightly when the particle size increased from the 22.6–32 mm to the 45–64 mm size-class, but dropping sharply for the coarser class (64–90.5 mm). Rates were 90% (85%–91% according to the injected year), 89% (76%–94%), 81% (76%–86%), 73% (50%–83%) for particle size-classes of 22.3–32 mm, 32–45 mm, 45–64 mm, and 64–90.5 mm, respectively. For particles injected into the banks, the mobilization rate is 100% because of the bank retreat that occurred between 2010 and 2020. If we consider individually the injection points (cluster or cross-section), the mobilization rates varied from 7% to 100%, the second lowest rate being relatively higher at 33% (Figure 4B). Lastly, we observed a net difference in mobilization rates according to the year, the type of geomorphic unit, or even the injection method (cluster or cross-section) of tagged particles. The general pattern was of higher rates for 2011 particles, for particles injected in pools, and for particles injected along cross-sections (Figure 3, Figure 4B).

4.2 2010-2020 bedload velocity

The mean and median velocity for all particles injected in the bed for all dates are 6.8 m y^{-1} and 2.9 m y^{-1}, respectively (Figure 5). Moreover, the velocity decreases with increasing grain-size: its mean

(median) is respectively 13 (7.1) m y^{-1}, 6.7 (4.6) m y^{-1}, 3.2 (1.6) m y^{-1}, and 1.1 (0.5) m y^{-1} for particle size-classes of 22.3–32 mm, 32–45 mm, 45–64 mm and 64–90.5 mm, respectively (Figure 6). In terms of individual injection points in the bed (cluster or cross-section), the mean and median velocities varied from 0.01 m y^{-1} to 14.2 m y^{-1} and from 0 m y^{-1} to 12.8 m y^{-1}, respectively (Figure 4C and D). The longitudinal pattern shows substantial variability but with slightly higher values along the upstream stretch of 230–300 m (Figure 6).

Furthermore, not unlike the mobilization rates, we observed important variability in the bedload velocity according to the year of injection, the type of geomorphic unit, and finally the method (cluster or cross-section) used to inject the tagged particles (Figure 4C, Figure 4D, Figure 5, Figure 6). As these observations are valid for all grain-size classes (taken individually or together), we go on to detail these points solely for the 22.6–32 mm size-class. We did so for clarity of purpose and because the velocity of particles belonging to this class and that of D_{50} can be deemed reasonably similar: whichever way the tagged particles are considered (by year or unit or method of injection), the mean and median grain-size for the 22.6–32 mm size-class of the detected particles ranged between 27 and 30 mm, which is very close to the bed surface D_{50} on the studied bend (28 mm).

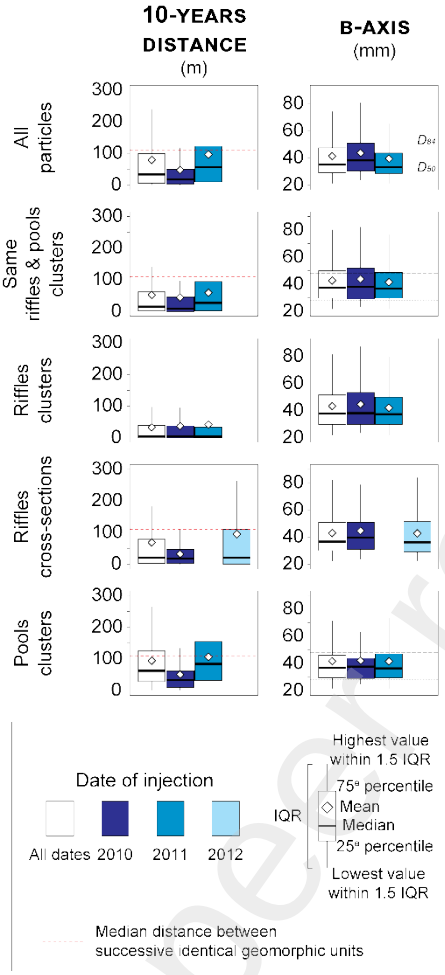

Figure 5 – Box-plots of 10-year distances and particle size for all particles grouped by date of injection, geomorphic unit and injection method.

First, the particles injected in 2010 were the slowest: their mean (median) velocity was 8.9 (3.1) m y^{-1} yet 9.5 (6.9) m y^{-1} for the 2011 ones, when focusing on particles injected in clusters on the same riffles and pools in both years. For the particles injected individually along cross-sections in riffles in 2010 and 2012, their velocity was 4.9 (2.1) and 18.8 (7.2) m y^{-1}, respectively (Figure 6). Second, the velocity of particles injected in pools was greater than that injected in riffles: for the 2010 particles, their velocity was 9 (1) m y^{-1} for the former versus 8.6 (5.7) m y^{-1} for the latter (Figure 6). The difference is more pronounced for the 2011 particles: 5.9 (1) m y^{-1} for the riffle particles versus 16.9 (16.3) m y^{-1} for the pool ones (when considering the same pools than in 2010, P1A and P2B; when considering all pools, as seen in Figure 6, the velocity is roughly the same: 17.5 (14.2) m y^{-1}). Lastly, particles injected along cross-sections moved faster than those injected in clusters (comparison only possible for riffles in 2010):

the mean (median) is 9 (1) m y^{-1} for the cluster particles and of 4.9 (2.1) m y^{-1} for the cross-section particles (Figure 6).

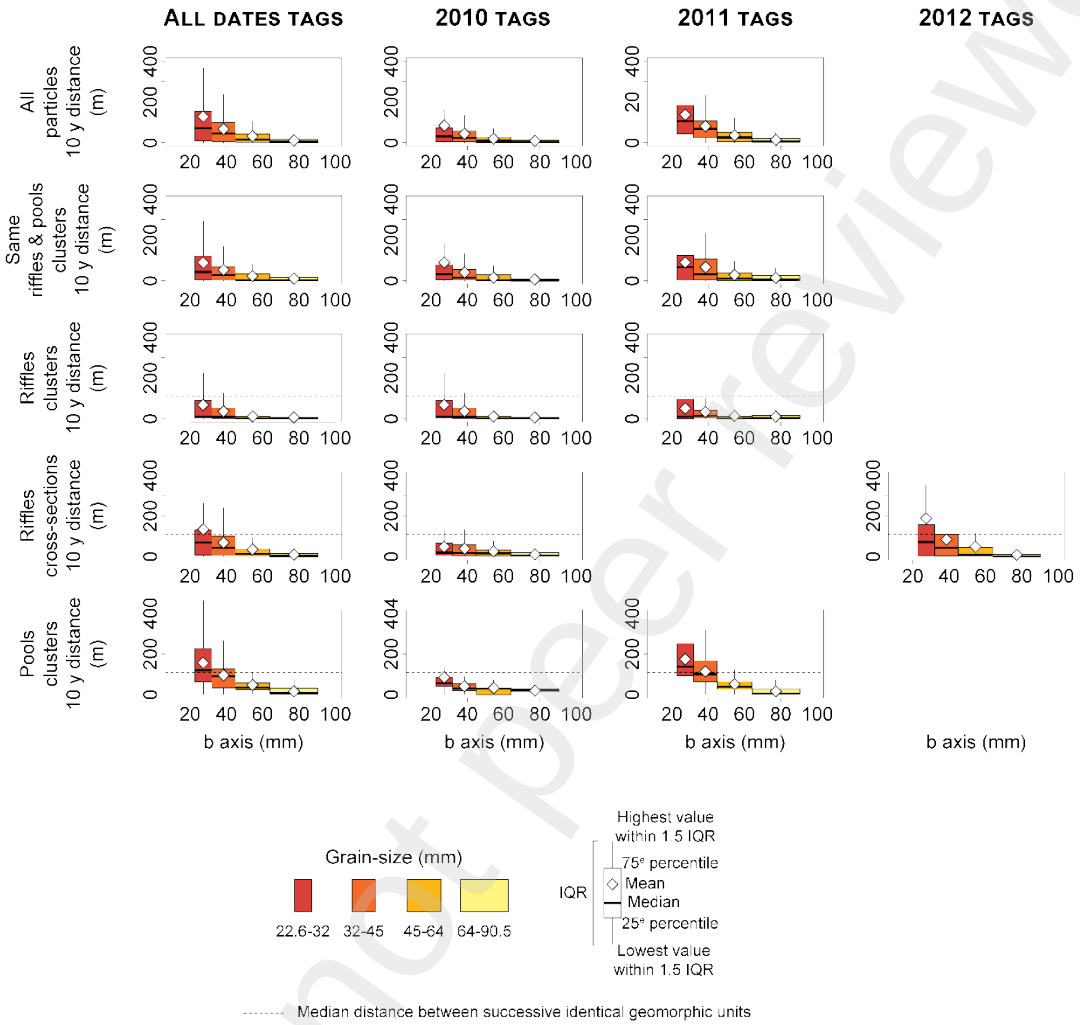

Figure 6 – Box-plots of 10-year distances for each half-phi class size.

For the clusters in banks (BT1 and BT2, cf. Figure 2), the velocity was higher for the 2011 particles and those coming from the downstream bank. Specifically, for the only two size-classes equipped with tags, the mean (median) velocity was 18.8 (13.8) m yr^{-1} for the 22.3–32 mm size-class but lower at 7.8 (3.6) m yr^{-1} for the 32–45 mm size-class. The velocity for the 22.3–32 mm size-class was similar for the 2010 and 2011 particles: 16.9 (14.2) versus 19.1 (13.7) m yr^{-1}), whereas for the 32–45 mm size-class, it is clearly higher in 2011: 9.7 (4.11) versus 5.2 (2.5) m yr^{-1}. Moreover, the velocity of particles was clearly lower for those injected into the upstream bank (BT1) than downstream bank (BT2): 13.2 (11.7) m yr^{-1}

versus 30.5 (16.2) m yr^{-1} for all particles and all dates. In comparison to particles injected into banks, the velocity of particles injected at the bank toe was lower for the 22.3–32 mm size-class (14.9 [7.2] m yr^{-1}), but higher for the 32–45 mm size-class (8.6 [6.3] m yr^{-1}). Regarding the 2011 particles injected into banks, they moved faster; however, the velocity of particles injected at the toe were higher for the upstream bank. In detail, the velocity for the 22.32 mm size-class is 15.8 (4.4) m yr^{-1} in 2010 and 13.9 (15) m yr^{-1} in 2011. For the 32–45 mm size-class, it was 7.9 (5) m yr^{-1} in 2010 and 9.4 (6.9) m yr^{-1} in 2011. The velocity of 22.3–32 mm particles injected at the toe of the upstream bank was 23.8 (16.7) m yr^{-1}. For the downstream bank, it was 8.2 (5.8) m yr^{-1}. For the 32-45 mm size-class, it was 12.7 (15.6) m yr^{-1} for upstream and 5.1 (4.9) m yr^{-1} for downstream.

4.3 2010-2020 bedload trajectory

For the study period, half of particles injected into the bed (particles injected at bank toe and in banks excluded) remained in their geomorphic unit of injection (Figure 7, Figure 8). On a per year basis, the retained proportions were 64%, 40%, and 55% for the 2010, 2011, and 2012 particles, respectively (Figure 7). The proportion of particles trapped in their geomorphic unit of injection increased with particle size, being 31%, 44%, 65%, and 80% for the 22.3–32 mm, 32–45 mm, 45–64 mm, and 64–90.5 mm size-classes, respectively. The individual trajectory of particles can be seen for each size-class in Figure 8. Furthermore, in 2020, the proportion of particles persisting in riffles surpassed that in pools (34%–50% for riffles versus 7% for pools), despite much shorter distances from the injection point to the exit units in riffles (mean, median of 21, 15 m for riffles versus 62, 69 m for pools) (Figure 7). For the 22.6–32 mm size-class (which encompasses D_{50}), most particles initially injected into pools were deposited outside of them (Figure 7). The difference in proportion between units decreased with particle size. Lastly, 80% of particles injected into the bed (particles injected at bank toe and in banks excluded) remained in their geomorphic unit of injection or in that located immediately downstream (Figure 7). By year, the retained proportions were 90%, 72% and 83% for 2010, 2011 and 2012 particles respectively (Figure 7). When examined by size-class, the proportions were 62%, 79%, 91%, and 99% for the 22.3–32 mm, 32–45 mm, 45–64 mm, and 64–90.5 mm classes, respectively.

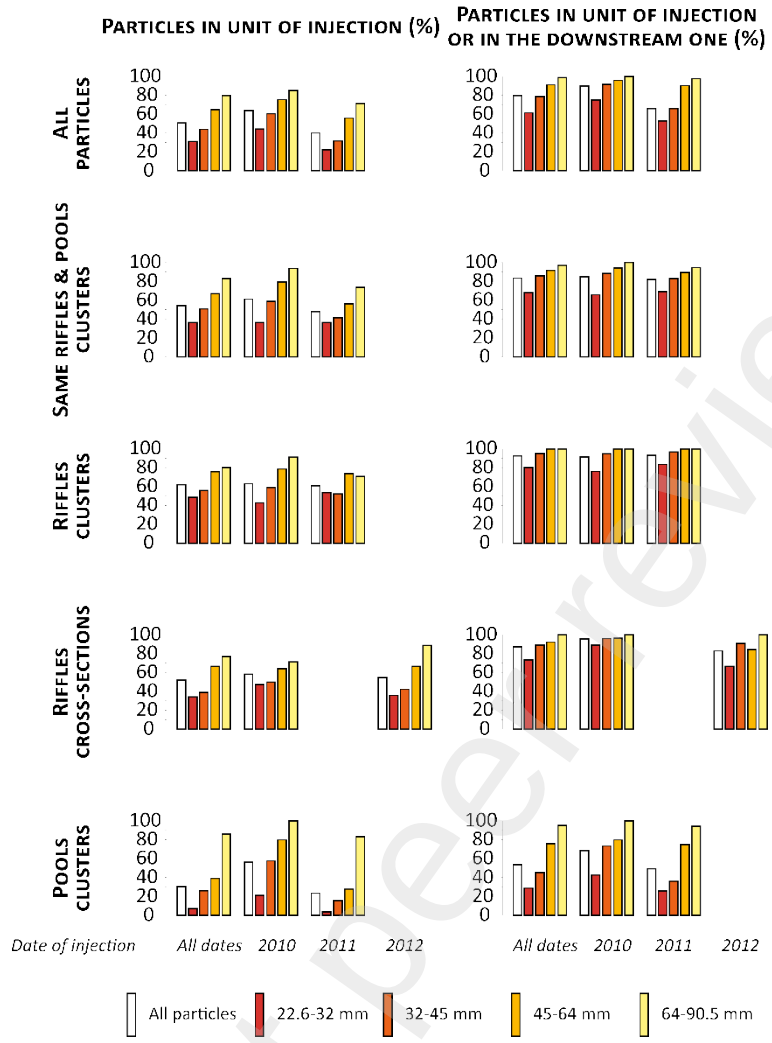

499

500 Figure 7 – Percentage of particles that remained in their unit of injection or deposited in the downstream

501 one in 2020.

502

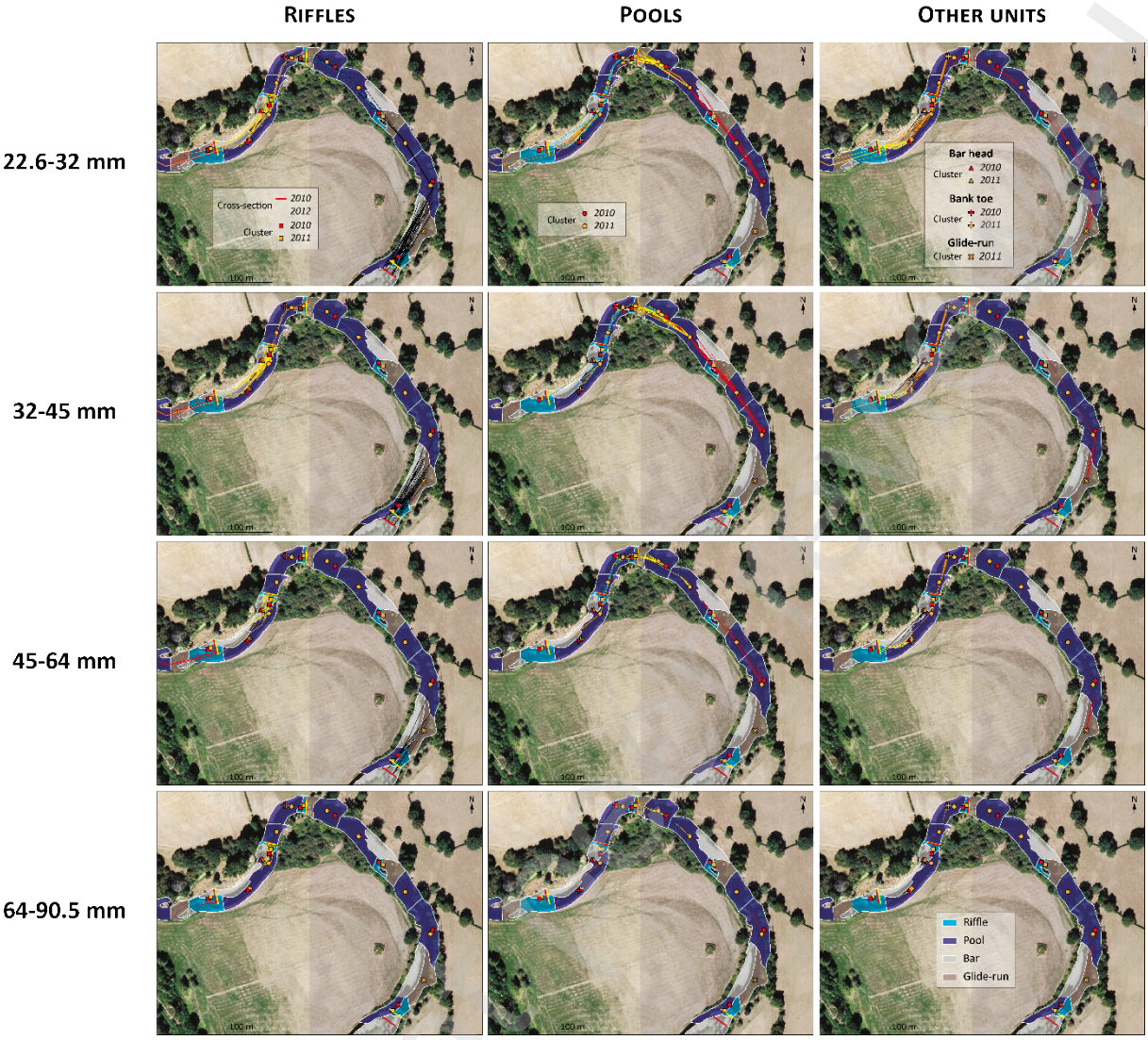

Figure 8 – Trajectory of individual tagged particles from 2010/2011/2012 to 2020.

The question of bedload trajectories was also addressed indirectly, by comparing the 10-year bedload velocity with the median distance between successive riffles and between successive pools (110 m). For all dates and particles injected into the bed, only 18% of particles travelled greater than the median distance between identical geomorphological units. By year, the proportions that did so were 7%, 23%, and 25% of the 2010, 2011, and 2012 particles, respectively; examined by size-class, it was 38%, 17%, 6%, and 0% for the 22.3–32 mm, 32–45 mm, 45–64 mm, and 64–90.5 mm classes, respectively. Moreover, for all dates and particles injected into the bed, only 37% of particles travelled a distance longer than half the median distance between identical geomorphological units. Detailed by year, that proportion was 21%, 46%, and 35% for the 2010, 2011, and 2012 particles, respectively. Examined by

size-class, it was 59%, 45%, 18%, and 2% for the 22.3–32 mm, 32–45 mm, 45–64 mm, and 64–90.5 mm classes, respectively.

Finally, we also characterized the influence of the laterally migrating bar (B4) on the trapping efficiency of particles at a decadal scale. For each geomorphic unit of tag injection upstream of the most active bar (all dates, cluster and cross-section taken together), we looked at the percentage of particles trapped in that bar. The Figure 9 shows that whether it be for all particles or only for the 22.3–32 mm size-class, the percentage of particles trapped in the B4 bar strongly decreased along the 100–120 m upstream of it; however, the influence of that bar on particle trapping then becomes null between 220 and 280 m upstream of it. Hence, the length scale of the bar B4's influence on bedload transport at a decadal period seems to not exceed 220–280 m. Furthermore, most particles injected at the bar head remained on the bar (92%). Finally, we looked at the percentage of 22.3–32 mm particles injected into the upstream active bank and at its toe that were deposited in the B4 bar. For particles in the bank, this bar trapped 36% of the tagged particles; for those at the bank toe, it trapped 44% of them. These values exceeded somewhat those reported for the particles injected in the surrounding geomorphic units (8% for S3, 25% for M3A, these located at the same cross-section as the cluster at the bank toe, and 33% for M3B).

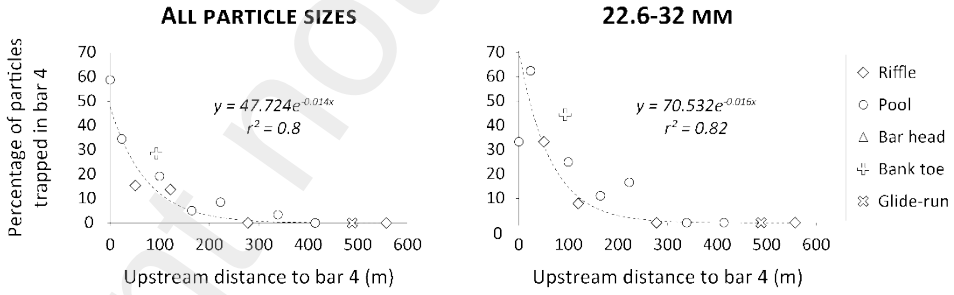

Figure 9 – Percentage of particles trapped in the bar B4 in 2020 in relation to the distance from the injection point to the bar head.

4.4 Velocity distribution

Whether we examine particles all together or by date of injection, the distribution of their path length was strongly right-skewed (Figure 10). The four probability distributions fitted—exponential, gamma, Pareto, and Weibull—described well the annual velocity distribution (Figure 10A). Based on the AIC,

539 the best fit was obtained by the Pareto distribution (Pareto type 2), except for the 2012 tags, where
540 gamma and exponential distributions appear better suited.

541 Finally, when the particles are differentiated by year of injection, the α and α_H values are
542 consistently < 2, indicating the strong likelihood of heavy-tail velocity distributions (for the 22.6–32
543 size-class: α between 1.08 and 1.75 with an R^2 of 0.74–0.94, and range of α_H between 0.9 and 1.6; for
544 all particle sizes: α between 1.12 and 1.75 with an R^2 of 0.74–0.93, and range of α_H between 0.99 and
545 1.81) (Figure 10B). When all years of injection are taken together, the discrimination between thin and
546 heavy tails was less clear in that most of α and α_H were slightly higher, even if relatively close, than 2
547 ((α = 2.12, R^2 = 0.86, and α_H = 1.75 for the 22.6–32 size-class; α = 2.18, R^2 = 0.84, and α_H = 2.02 for
548 all particle sizes) (Figure 10B).

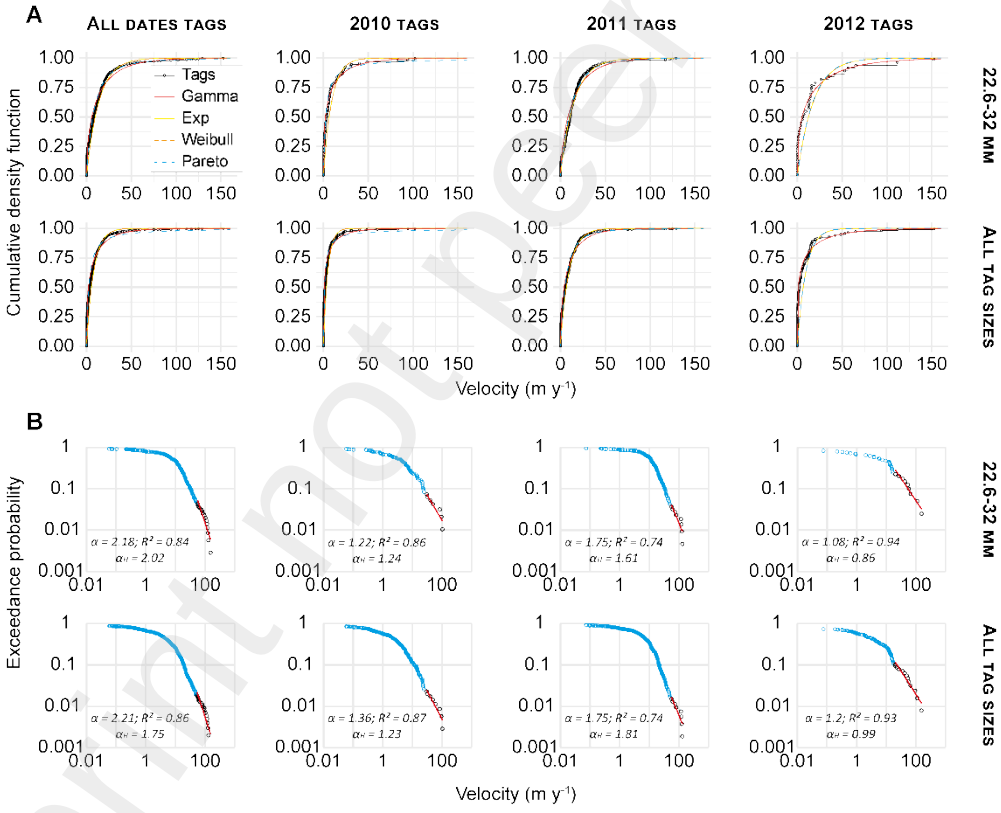

549

550 Figure 10 – Cumulative density function of annual velocities fitted with fitted exponential, gamma,
551 Pareto, and Weibull distributions (A); Exceedance probability plots of annual velocities with α and α_H
552 values of the tail's distributions (tails are plotted in black) (B).

553

554

555 **4.5 Estimation of event and long-term bedload velocity**

556 For the whole discharge record (1988–2020) at the reference gauging station of Montluçon, 154
557 competent events (50 events per decade) occurred, with a mean duration of 7 days per event (Figure
558 11). Full mobility is theoretically reached at 137 $m^3 s^{-1}$ and 176 $m^3 s^{-1}$ (corresponding to return intervals
559 of 3 years and 6 years, computed according Gumbel's adjustment of annual maximum discharges) when
560 estimated from τ_m^* and τ_c^*, respectively (Figure 11). This happened for 14 and 9 events from 1988 to
561 2020, respectively (Figure 11).

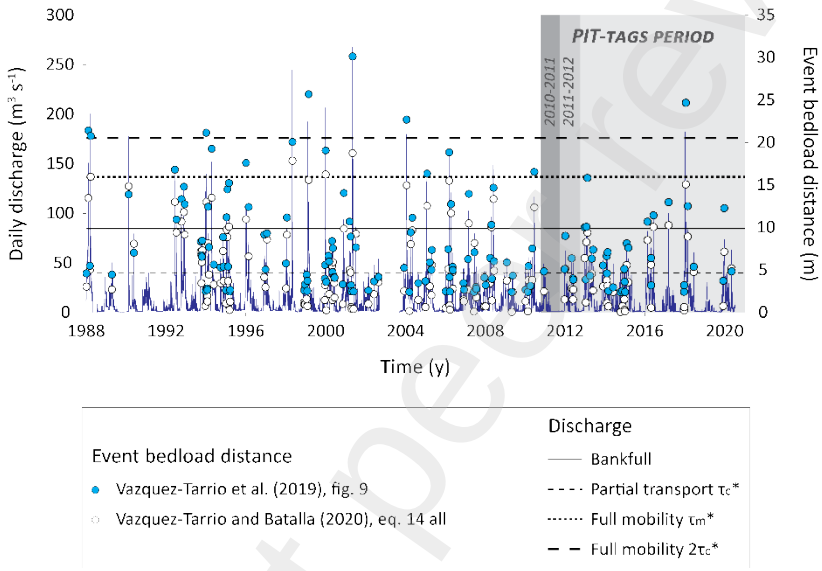

562

563 Figure 11 – Reconstruction of the mean event bedload distances for D_{50} from 1988 to 2020.

564

565 Comparing the actual distance travelled by the bed D_{50} from tag tracking (22.6–32 mm size-
566 class) to that predicted by recent formulas in the literature shows a relatively good agreement for those
567 of figure 9 in Vázquez-Tarrío et al. (2019) (here, formula D in Figure 12Figure 11) and for all types of
568 rivers [eq. 14] in Vázquez-Tarrío and Batalla (2019) (here, formula D in Figure 12). This was verified
569 for annual transport distance in 2010–2011, though to a lesser extent than in other periods, namely 2011–
570 2012 and the longer periods of 2010–2020, 2011–2020, and 2012–2020 (Figure 12).

571

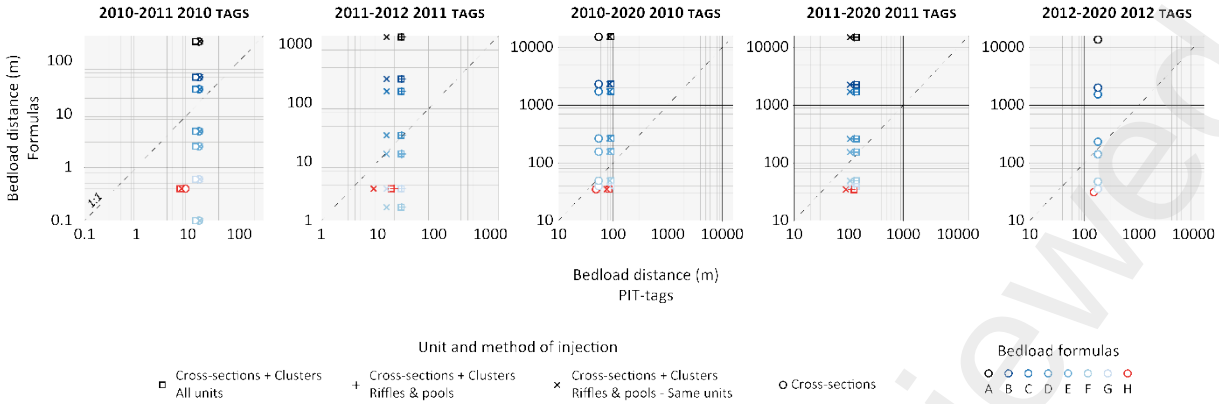

572

573 Figure 12 – Mean bedload distance (m) between 2010 and 2020 estimated using bedload formulas
574 (with critical discharge values of 40 $m^3 s^{-1}$ and 50 $m^3 s^{-1}$) and PIT-tags tracking. The distances were
575 obtained from mobilized and non-mobilized particles for all formulas, with the exception of formula H
576 that computes distances from mobilized particles only. In bold, the distances obtained from formulas
577 that are closest to the empirical tag distances. CSs: cross-sections. Cs: clusters.
578 A: Vázquez-Tarrío and Batalla (2019), eq. 13. B: Vázquez-Tarrío et al. (2019), eq. for riffle-pool rivers
579 in figure 4 for riffle-pool rivers. C: Vázquez-Tarrío et al. (2019), eq. in figure 2 for riffle-pool rivers
580 with width/depth bankfull ratio > 10. D: Vázquez-Tarrío et al. (2019), eq. for all rivers except the step-
581 pool ones of figure 9. E: Vázquez-Tarrío and Batalla (2019), eq. 14 for all rivers. F: Vázquez-Tarrío and
582 Batalla (2019), eq. 14 for riffle-pool rivers. G: Vázquez-Tarrío and Batalla (2019), eq. 15 for riffle-pool
583 rivers. H: Gilet et al. (2020), eq. 4.
584
585 These comparisons revealed that both formulas were well able to reconstruct the transport
586 distances of D_{50} at the competent event scale on the studied bend. Between 1988 and 2020, the mean
587 and median event distances for the 154 events that occurred were respectively 5.6 m and 7.7 m when
588 using the formula D, and likewise 3.3 m and 5.1 m when using formula E. Of all events, 90% had a
589 distance less than 12.2-15.7 m. The maximum distance was 18.8 m and 30.2 m under formula D and E,
590 respectively, being equal or lower than the active channel width and 5.9–3.6 times lower than the median
591 distance between riffles and between pools. The maximum distance attained was for a 31-day-long
592 event, whose discharge was the highest during the study period (with a 34-year return interval period,
593 computed according Gumbel's adjustment of annual maximum discharges) and for which the ratio

τ^*/τ_c^* was equal to 2.3. Not one of the 9–14 events for which full mobility occurred was thus able to transport bedload on a distance equivalent to the distance between identical successive geomorphic units. Even when applying the formulas to a fictional 10-day duration event with a constant 100-year return interval discharge (321 m^3 s^{-1}) yielded very low distances: 22 m for formula D and 20 m for formula E. Finally, extrapolating the cumulative distance obtained for the 1988–2020 period to a duration of one century yielded an average long-term velocity of 2.5–3.8 km $century^{-1}$.

5. Discussion

5.1 Variability in bed mobility and bedload velocity according to the year, type of geomorphic unit, or method of injection

Our results show there is important variability in both bed mobility and bedload velocity according to the year, geomorphic unit type (and between units of the same type), and injection method (in cluster or along cross-section) Understanding the reasons for such a discrepancy is a crucial issue in the context of trying to obtain reliable bedload velocities.

Regarding the variability between particles injected in riffles versus pools, this could arise from a difference in the available energy between these two types of units. According to the concept of hydraulic reversibility, the average velocities and shear stresses during high flow should be higher in pools (Booker et al., 2001; Caamano et al., 2009; Keller, 1971; Keller and Florsheim, 1993; Lisle, 1979; MacWilliams Jr. et al., 2006; Milan et al., 2001; Petit, 1987; Thompson, 2011; Thompson et al., 1999). Yet that process is not universal: it may only occur when the wetted cross-sectional area of riffles exceeds that of pools (Carling, 1991; Clifford and Richards, 1992; Milan, 2013; Milan et al., 2002; Thompson, 2011; Wilkinson et al., 2004), a situation rather infrequent (Carling and Wood, 1994; Thompson, 2011; Thompson et al., 1999). For example, from a set of 702 pool-riffle couplets across northern California, Byrne et al. (2021) found that reversal occurs at the bankfull for only 18% of all couplets. The higher mobility of material in pools is perhaps more likely the result of the existence at high-flow of convergent and jet flow at the entrance and centre of pools, respectively, and of divergent and uniform flow at the pool tail and in riffles, respectively (e.g., MacWilliams Jr. et al., 2006;

Thompson and MacVicar, 2020). Furthermore, bed mobility and velocity could be promoted for tracers injected into forced pools, namely for four of the seven pools equipped in our study (i.e., P1B, P2B, P3A, P3B). In such units, the constriction imposed by the crosswise physical obstacles reinforced the convergence of flows, and in such circumstances the flows near the bed surface are generally associated with high turbulence (Hassan and Woodsmith, 2004; MacVicar and Roy, 2007a, 2007b, 2011; Thompson, 2007; Thompson and Wohl, 2009). When tracers are injected in the deepest sections of the forced pools, as done in our study, mobility is reportedly higher than in riffles (Thompson and Wohl, 2009; MacVicar and Roy, 2011). Yet our data do not show such an effect of forced pools: for each pair of unforced–forced pools (M1A–M1B, M2A–M2B, M3A–M3B), the velocity was either higher or similar for particles injected in the unforced pool. The difference between forced and free-formed pools could nonetheless result from lower distances travelled through pools for particles injected in the former (24 m, 38 m, and 21 m from the injection point to the exit of the forced pools M1B, M2B, and M3B, respectively, versus 103 m, 87 m, and 69 m for the free-formed pools M1A, M2A, and M3A, respectively). Furthermore, the lateral location of clusters can also explain, at least in part, the difference in bed mobility and bedload velocity observed between riffles and pools. Whereas clusters in pools were systematically located in the their central deepest section, where the jet flow is supposed to occur, three of the five riffle clusters (R2, R3, and R5) were located in the bend and not at the inflexion point (R1 and R4), where the clusters were positioned rather than in the inner half of the bed, where the flow velocity could be relatively low. This explanation is supported by the clearly lower bed mobility and bedload velocity of tracers injected in these three riffles compared with the two remaining riffles (range of mobilization rate: 7%–72% for R2, R3, and R5 versus 93%–100% for R1 and R4; respective ranges of mean, median velocity: 0.8–4.9 m y^{-1}, 0–0.3 m y^{-1} versus 3.8–8.2, 0-–0.3 m y^{-1} and 3.2–6.8, 0–0.3 m y^{-1}). When compared with pools, the mobilization rate as well as bedload velocity of these three riffles (R2, R3, R5) are also clearly lower, but similar for the two remaining riffles. In addition, sedimentological arguments can also be put forward. Some research demonstrated that the structure of the surface layer of pools (their degree of packing especially) is clearly less stable than for riffles (e.g., Clifford, 1993; Hodge et al., 2013; Sear, 1996). Further, during low flow, the competence in riffles surpasses that in pools (Milan et al., 2002): the finest fraction of the bedload, sand, and small gravel, is

649 at least partly exported from the former and accumulated in the latter (Jackson and Beschta, 1982; Lisle
650 and Hilton, 1992, 1999; Milan, 2013; Sear, 1996). The pools are thus frequently lined with a more or
651 less thick layer of fine material and the sand content in their subsurface layer could be more important
652 than in riffles. This may have been a factor contributing to greater bed mobility in pools (Sear, 1996;
653 Vahidi et al., 2020). Work by Curran and Wilcock (2005), Wilcock (1998) or Wilcock and Crowe
654 (2003), for example, show that significant increases in the mobility of gravel occur when the proportion
655 of sand in the bed increases. All the possible explanations presented above are theoretically valid at the
656 scale of the competent events, or so long as tracers remain in their unit of injection. Over time, given
657 the tracers' alternating passage through riffles and pools, the discrepancy in velocity should eventually
658 slow to zero. When considering only those tracers that left their unit of injection, we still found a marked
659 difference in bedload velocity between tracers seeded in riffles and in pools: for 2010 tracers, mean
660 (median) of 11 (5.6) m y^{-1} and of 9.6 (6.7) m y^{-1} for riffles and pools, respectively; for 2011 tracers,
661 mean-median of 8.1 (6.3) m y^{-1} and 13.7 (12.6) m y^{-1} for riffles and pools, respectively. This shows that
662 the effect on the bedload velocity from the type of unit that received the injection can persist 10 years
663 after the injection. This most likely arose from the low bedload velocity reported: half of the tracers
664 remained in their unit of injection (31% for the 22.6–32 mm size-class) and 80% of tracers were
665 deposited in their unit of injection or in the downstream one (62% for the 22.6–32 mm size-class) (Figure
666 7). Secondly, it is also probably reflects the effect from the difference in distance from injection points
667 to the exit of a geomorphic unit according to its type. This distance is clearly shorter in riffles than pools;
668 mean (median) of 21 (15) m versus 62 (69) m, and references back to the proportions leaving the two
669 types of units. However, lacking detailed data on the hydraulic functioning and surface sediment
670 structure of these units, which of the above potential explanations—for the difference in velocity
671 between particles injected in riffles versus pools—is prominent cannot be known.

672 The lower velocity of particles injected as clusters than along cross-sections likely originates
673 from the bed mobility's laterally discrete nature. For partial transport events, namely for most of the
674 competent events, only a portion of the bed cross-section, which expands with the flow strength, is
675 indeed mobile (Ferguson, 2003; Frings and Vollmer, 2017; Haschenburger, 2017; Haschebburger and
676 Wilcock, 2003; Papangelakis and Hassan, 2016). Injections performed in a cluster would thus provide

an under-estimation of the bedload velocity when the cluster is positioned on a rarely active portion. Conversely, that velocity could be overestimated if the cluster is located on a frequently active part of the bed. Broadly then, injecting along a cross-section would let us incorporate the lateral variability of bed mobility and thus yield a more representative image of bedload velocity.

In order to integrate the effects of these different sources of variability for bed mobility—that is laterally, between types of geomorphic units, as well as between units of the same type) —thereby obtain the most reliable bedload velocity possible, we recommend using seed tracers in several equidistant clusters along cross-sections, with a least two or three particles of each half-phi grain-size per cluster. Such injections should be made in several riffles and in several pools, with cross-sections systematically located at the same relative longitudinal position (i.e., heads of riffles and centres of pools, for example). Whatever the chosen injection design, the variability in bedload velocity should lessen over time and be paramount when full mobility is rare.

The inherent spatial variability of bed mobility and velocity could also explain, in part, the lower mobility and velocity observed for 2010 tags vis-à-vis 2011 and 2012 to the extent that particles were injected at a slightly different position in a given year versus others. Operator bias is very likely negligible, in that particles were injected in the same way and by the same person. The last potential explanation is related to the differing flow history between tracers: because 2010 and 2011 tracers share the same hydrology following the injection of 2011 tracers, an explanation for the lowest decadal velocity of the 2010 tracers could theoretically lie in what happened before the injection of the 2011 tracers. Indeed, the 2010 tracers underwent a very long low flow period prior to the 2011 tracers' injection (Figure 11), that could generated a rearrangement of the surface structure that led to its strengthening, thus limiting the particles' mobility. Numerous authors have highlighted the fundamental role of stress history, that is to say sub-critical shear stresses, in strengthening the surface layer stability (Haynes and Pender, 2007; Monteith and Pender, 2005; Ockelford and Haynes, 2013; Paphitis and Collins, 2005). The effect of such limitations for the 2010 tracers' mobility should have emerged in the 2010–2020 period, and accordingly, in 2011–2012, the 2010 tracers ought to have moved slower than the 2011 tracers. Yet the opposite occurred. When comparing tracers introduced in clusters to the same units (pools or riffles) in both years, the mean velocity of the 22.6–32 mm size-class is 12.9 m y^{-1} and

5.4 m y^{-1} for the 2010 and 2011 tracers, respectively. Further, whereas the total expenditure of flow energy for a discharge higher than the critical discharge (*sensu* Haschenburger, 2011a) was 9.4 times lower in 2010–2011 than 2011–2012, the mean virtual velocity (distance divided by the duration of competent discharge) of the 22.6–32 mm size-class was clearly higher for the 2010 tags in 2010–2011 than the tags 2011 in 2011–2012 (69.4 mm h^{-1} versus 7.3 mm h^{-1}). We conclude the difference in the location of the tracers' injection between years is the only satisfactory explanation for the variability in velocity between years.

5.2 Interactions between event bedload distances and bedforms

For the entire period of recorded discharge (1988–2020), despite the occurrence of 9–14 events for which the full mobility was reached, the maximal estimated mean event distance for the D_{50} was 30.2 m. This is roughly equivalent to the active channel width and 3.6 times less than the median distance between riffles and between pools. The main implications for the Cher River, and perhaps more broadly for temperate low-energy gravel-bed rivers, are twofold. First, event transport distances would be always, or almost always, shorter than the distance between two successive identical geomorphic units. It implies that trapping effect by bars would be rare, or even absent, at the scale of competent events for most of particles located at a distance higher than an active channel width. Second, since no event is able to transport bedload on distances at least equal to the length of a single riffle-pool unit, the maintenance of bedforms, and especially that of bars, would thus become disconnected from the event transport distances or would depend on successive minor changes. Therefore, the model proposed by Pyrce and Ashmore (2003) would not be universally valid. When computing the cumulative distance of D_{50} for events whose peak is higher or lower than the bankfull discharge, we see that events below the bankfull are responsible for about half of the total distance for the 1988–2020 period. By setting the threshold to a 2-year return interval flood, events with lower discharge than that are responsible for ca. 70% of the total distance for the 1988–2020 period. This agrees with and supplements the findings of Dépret et al. (2015) along the same reach on which the study bend is located, showing that its morphogenesis, from the perspective of planform mobility and effective discharge for the bedload, is chiefly controlled by low-magnitude hydrological events (< 2 years RI).

Finally, the possibility remains that the study bend's current bed morphology could be maintained by very rare floods and/or had been inherited from a past flood regime. Still, along those scarce sections of the Cher River whose geometry has freely adjusted over the last decades (due to the lack of lateral constraints), there exists riffle–pool–bar sequences with length scales of bedforms similar to that in the study reach. This suggests the present morphology can be maintained under the current flood regime, and without the occurrence of a very rare flood event.

5.3 Long-term bedload estimation

The range of long-term bedload velocity we proposed here is an overestimate for two key reasons. First, the study bend's hydraulic parameters are not representative of the whole 12-km long reach, which ends at the junction with the Aumance River (see Dépret et al., 2015, 2017 for details) and is where the bend is located. Although their active channel width is similar, the low-flow bed slope is equal to 0.00063 m m^{-1} along the reach, versus the greater 0.0011 m m^{-1} along the study bend, where the bankfull stream power is thus almost two times higher (30 W m^{-2} versus 17 W m^{-2}). This implies the long-term velocity should be derived instead from the hydraulic parameters of the reach. By doing so, the application of formulas D and E using hydraulic parameters of the reach provides velocities of 0.95 and 1.3 km $century^{-1}$, respectively (versus 3.8 and 2.5 km $century^{-1}$ for the study bend). Secondly, it is very likely that our estimation takes into account, only partially, the progressive slowdown of the tracers resulting from their mixing within the event active layer (*sensu* Church and Haschenburger, 2017), or their trapping in bars or in the floodplain (Ferguson et al., 2002; Ferguson and Hoey, 2002; Haschenburger, 2011a, 2011b; Houbrechts et al., 2015; Iwasaki et al., 2018; Pelosi et al., 2016). For example, in the Carnation Creek, Haschenburger (2011a) reported that a 72% reduction in velocity after a few years, which reached then an asymptotic value. In the Allt Dubhaig, Ferguson et al. (2002) found a 50% reduction in velocity when comparing it 2 years and 8 years following the tracer injection. Here, long-term bedload velocity in the Cher River was estimated through formulas that succeeded in reconstructing the tracers' velocity at a 10-year scale. Yet, because of the low transport distances reported, we find that only a small proportion of all tracers could have been affected by the trapping effect of bars on this time scale. Such a weak effect is also evident in the similar velocity of tracers deposited on and outside the bar B4: respectively

761 having a mean (median) of 8 (5.3) and 8.1 (3.8) m y^{-1} for all particles; likewise, 13.6 (8.7) and 14.7 (10)
762 m y^{-1} for the 22–32 mm size-class. Furthermore, especially because of relatively weak hydrologic
763 activity during the 10-year study period, coupled with river's inherently low energy, it is likely that the
764 mixing process of tracers into the active layer was still incomplete at 10 years since their injection. In
765 this respect, Haschenburger (2011a) showed, for example, that large floods accelerate the rate at which
766 the vertical mixing of surface tracers occurs. Recently, Vázquez-Tarrío et al. (2021) highlighted that, at
767 the event scale, the ratio between the Shields stress for the peak flow and the critical Shields stress is
768 one of the main drivers of the active layer's depth. By comparing the virtual velocity (i.e., total distance
769 divided by the total duration of competent events) of tracers 1 year and 10 years following their injection,
770 we could indirectly gain insight into the intensity of their mixing process, the idea being that the smaller
771 the difference, the weaker is the mixing. For the 2010 tracers, the mean virtual velocity of the 22.6–32
772 mm size-class was much faster in the 2010–2011 period than 2010–2020 period (74 mm h^{-1} versus 13
773 mm h^{-1}, a 82% decrease). Yet, when comparing the median velocity, the velocity is higher for the longest
774 period (5 mm h^{-1} versus 3 mm h^{-1}, a 148% increase). We find a similar tendency for the 2011 tracers,
775 but with a clearly smaller difference for the mean (24 mm h^{-1} for the 2011–2012 period versus 20 mm
776 h^{-1} for the 2011–2020 period, a 15% decrease; for the median, 8 mm h^{-1} versus 15 mm h^{-1}, a 198%
777 increase). Hence, it seems virtual velocity has not or only marginally decreased with elapsed time. This
778 would tend to confirm a weak mixing of tracers in the active layer. The right-skewed distribution of the
779 bedload velocity and its likely heavy-tail (Figure 10) further support this interpretation of a mixing
780 having yet not reached its equilibrium. Both features, which could serve as a signature of a super-
781 diffusive regime of the bedload (Lajeunesse et al., 2013), would stem from the fact that a crucial
782 proportion of them remains overly mobile so long as they have not been fully mixed into the active layer
783 (Pelosi et al., 2016; Pierce and Hassan, 2020; Wu et al., 2019; Zhang et al., 2012). On a longer time-
784 scale, after the mixing has been achieved, the dispersion regime of the tracers would tend to become
785 diffusive, rendering their distribution of velocities more normal, with their variance increasing linearly
786 with time and their velocity becoming asymptotic (Guillon, 2016; Lajeunesse et al., 2018; Wu et al.,
787 2019; Zhang et al., 2012). But there is no consensus yet concerning the anomalous or normal character
788 of the dispersion of tracers in the long-term. Accordingly, Pierce and Hassan (2020) suggested that on

long time-scale—a geomorphic range as they called it—the regime would remain anomalous, for which superdiffusion or subdiffusion happens in a way that depends on the long-time decay of the exhumation time distribution of buried particles.

6. Conclusion

This paper focused on characterizing the variability of bed mobility in a low-energy, gravel-bed meandering river, with particular attention paid to the relationship between bed transport distances and bed forms. Our combined analysis of 10-years of data for tracked PIT-tags and a 32-year reconstruction of bedload distance events during which full mobility was reached on several occasions reveals a substantial slowness of the bedload in the studied river. Our findings highlight two take-home messages. First, the trapping effect by bars is rare, or even absent, at the scale of competent events for most of particles located at a distance greater than an active channel width from the bar. Second, since no event is able to transport bedload over distances at least equal to the length of one riffle-pool unit, the maintenance of bedforms, and especially of bars, would be disconnected from the events' transport distances or would result from successive minor changes. These findings do not support the hypothesis of Pyrce and Ashmore (2003a, 2005) claiming that, for full mobile events, bedload should be transported on distances at least equal to the distance between two successive bars, equivalent to the length of a riffle-pool unit, and that bedform maintenance depends on such events. More field and flume experiments should now be undertaken to check our results and to better understand the suite of conditions allowing the coexistence of an active, well-developed riffle-pool-bar morphology and low bedload distances during full mobility events.

Further, we uncovered evidence for considerable decadal-scale variability in the bedload velocity obtained from tracers according to the year of injection, the type of geomorphic unit that got injected, or the method of injection (cluster or cross-section). This emphasises why it is imperative to systematically consider the moment, location, and way tracers are seeded for the sound inference and interpretation of bedload velocity. In addition to exemplifying the well-known strong spatiotemporal variability of bedload processes, our results also highlight persistent effects upon velocity estimation from where, when and how tracers are injected, especially for low-energy rivers.

Lastly, our PIT-tags survey provides new empirical data on the long-term dispersion of surface seeded tracers at the decade temporal scale, this rarely documented in the literature, even less for low-energy rivers (Bradley, 2017; Haschenburger, 2011a, 2013; McDowell and Hassan, 2020; Papangelakis and Hassan, 2016). The right-skewed and heavy tailed velocity distribution reported here could indicate a very incomplete mixing of tracers within the active layer. The vertical diffusion of tracers in such low-energy rivers could therefore clearly be a more time-consuming process than previously reported for the few rivers documented to date (Haschenburger, 2011b, 2012). Consequently, the long-term bedload velocity estimation we gleaned from the PIT-tags data and bedload formulas should be viewed as strongly overestimated. This pinpoints the difficulty in (1) obtaining robust information on the way of, and velocity at which, the processes of advection-diffusion of the bedload occur in the long-term; and (2) extrapolating to long-term velocities from the PIT-tags velocities recorded over just a few years.

Acknowledgements

This research was conducted in the framework of the *Plan Loire Grandeur Nature*. It was funded by the FEDER *Bassin de la Loire*, the *Agence de l'Eau Loire-Bretagne*, and the *Zone Atelier Loire*.

References

Andrews ED, Nankervis JM. 1995. Effective discharge and the design of channel maintenance flows for gravel-bed rivers. In: Costa, J.E., Miller, A.J., Potter, K.W., Wilcock, P.R. (Eds.), Natural and Anthropogenic Influences in Fluvial Geomorphology. American Geophysical Union, Washington D.C., pp. 151-164.

Arnaud, F., Piégay, H., Vaudor, L., Bultingaire, L., Fantino, G., 2015. Technical specifications of low-frequency radio identification bedload tracking from field experiments: differences in antennas, tags and operators. Geomorphology 238, 37-46.

Ashmore, P.E., Church, M., 1998. Sediment transport and river morphology: A paradigm for study. In: Klingeman, P.C., Beschta, R.L., Komar, P.D., Bradley, J.B. (Eds.), Gravel-bed Rivers in the Environment. Water Resources Publications: Highlands Ranch, Colorado, pp. 115-148.

Baker, V.R., 1977. Stream-channel response to floods, with examples from central Texas. Geological Society of American Bulletin 88 (8), 1057-1071.

Beechie, T.J., 2001. Empirical predictors of annual bed load travel distance, and implications for salmonid habitat restoration and protection. Earth Surface Processes and Landforms 26, 1025-1034.

Booker, D.J., Sear, D.A., Payne, A.J., 2001. Modelling three-dimensional flow structures and patterns of boundary shear stress in a natural pool-riffle sequence. Earth Surface Processes and Landforms 26, 553-576.

Bradley, D.N., 2017. Direct observation of heavy-tailed storage times of bed load tracer particles causing anomalous superdiffusion. Geophysical Research Letters 44, 12,227–12,235.

Bradley, D.N., Tucker, G.E., 2012. Measuring gravel transport and dispersion in a mountain river using passive radio tracers. Earth Surface Processes and Landforms 37, 1034-1045.

Buffington, J.M., Lisle, T.E., Woodsmith, R.D, Hilton, S., 2002. Controls on the size and occurence of pools in coarse-grained forest rivers. River Research and Applications 18, 507-531.

Buffington, J.M., Montgomery, D.R., 1999. Effects of sediment supply on surface textures of gravel-bed rivers. Water Resources Research 35 (11), 3523-3530.

Byrne, C.F., Pasternack, G.B., Guillon, H., Lane, B.A., Sandoval-Solis, S., 2021. Channel constriction predicts pool-riffle velocity reversals across landscapes. Geophysical Research Letters, 48, e2021GL094378.

Caamaño, D., Goodwin, P., Buffington, J.M., Liou, J.C.P., Daley-Laursen, S., 2009. Unifying criterion for the velocity reversal hypothesis in gravel-bed rivers. Journal of Hydraulic Engineering 135 (1), 66-70.

Carling, P., 1991. An appraisal of the velocity-reversal hypothesis for stable pool-riffle sequences in the River Severn, England. Earth Surface Processes and Landforms 16, 19-31.

Carling, P., Wood, N., 1994. Simulation of flow over pool-riffle topography: A consideration of the velocity reversal hypothesis. Earth Surface Processes and Landforms 19, 319-332.

Carson. M.A., Griffith, G.A., 1989. Gravel transport in the braided Waimakariri River: Mechanisms, measurements and predictions. Journal of hydrology 109, 201-220.

873 Chapuis, M., Bright, C.J., Hufnagel, J., MacVicar, B., 2014. Detection ranges and uncertainty of passive
874 Radio Frequency Identification (RFID) transponders for sediment tracking in gravel rivers and
875 coastal environments. Earth Surface Processes and Landforms 39 (15), 2109-2120.
876 Church, M., 2006. Bed material transport and the morphology of alluvial river channels. Annual Review
877 of Earth and Planetary Sciences 34, 325-354.
878 Church, M., Haschenburger, J.K., 2017. What is the ‘‘active layer’’? Water Resources Research 53, 5–
879 10.
880 Church, M., Hassan, M.A., 2002. Mobility of bed material in Harris Creek. Water Resources Research
881 38 (11), 1237.
882 Church, M., Hassan, M.A., Wolcott, J.F., 1998. Stabilizing self-organized structures in gravel-bed
883 stream channels: field and experimental observations. Water Resources Research 34, 3169-3179.
884 Church, M., Mclean, D.G., Wolcott, J.F., 1987. River bed gravels: Sampling and analysis. In: Thorne,
885 C.R., Bathurst, J.C., Hey, R. (Eds.), Sediment transport in gravel-bed rivers. Wiley & Sons,
886 Chichester, pp. 43-79.
887 Clifford, N.J., 1993. Differential Bed Sedimentology and the Maintenance of Riffle-pool Sequences.
888 Catena 20, 447-468.
889 Clifford, N.J., Richards, K.S., 1992. The reversal hypothesis and the maintenance of pool-riffle
890 sequences: A review and field appraisal. In: Carling, P.A., Petts, G.E. (Eds.), Lowland floodplain
891 rivers: Geomorphological perspectives. Wiley & Sons, Chichester, pp. 43-70.
892 Curran, J.C., Wilcock, P.R., 2005. Effect of sand supply on transport rates in a gravel-bed channel.
893 Journal of Hydraulic Engineering 131 (11), 961-967.
894 Delignette-Muller, M.L., Dutang, C., 2015. fitdistrplus: An R Package for Fitting Distributions. Journal
895 of Statistical Software 64 (4), 1–34.
896 Dépret, T., 2014. Fonctionnement morphodynamique actuel et historique des méandres du Cher. Ph.
897 Thesis, Paris 1 – Panthéon-Sorbonne University.
898 Dépret, T., Gautier, E., Hooke, J., Grancher, D., Virmoux, C., Brunstein, D., 2015. Hydrological controls
899 on the morphogenesis of low-energy meanders (Cher River, France). Journal of Hydrology 531,
900 877–891.

Dépret, T., Gautier, E., Hooke, J., Grancher, D., Virmoux, C., Brunstein, D., 2017. Causes of planform stability of a low-energy meandering gravel-bed river (Cher River, France). Geomorphology 285, 58–81.

Dietrich, W.E., Kirchner, J.W., Ikeda, H., Iseya, F., 1989. Sediment supply and the development of the coarse surface layer in gravel-bedded rivers. Nature 340, 215-217.

Direction Départementale de l'Allier, 1998. Plan de Prévention du Risque Inondation du Val de Cher.

Downs, P.W., Soar, P.J., 2021. Beyond stationarity: influence of flow history and sediment supply on coarse bedload transport. Water Resources Research 57(2), e2020WR027774.

Eaton, B.C., Lapointe, M.F., 2001. Effects of large floods on sediment transport and reach morphology in the cobble-bed Sainte Marguerite River. Geomorphology 40, 291-309.

Einstein, H.A., 1937. Bed load transport as a probability problem. PhD Dissertation, Federal Institute of Technology, Zurich.

Ferguson, R.I., 2003. The missing dimension: effects of lateral variation on 1-D calculations of fluvial bedload transport. Geomorphology 56, 1 –14.

Ferguson, R.I., Bloomer, D.J., Hoey, T.B., Werrity, A., 2002. Mobility of river tracer pebbles over different timescales. Water Resources Research 38 (5), 1045.

Ferguson, R.I., Hoey, T.B., 2002. Long-term slowdown of river tracer pebbles: Generic models and implications for interpreting short-term tracer studies. Water Resources Research 38 (8), 1142.

Frings, R.M., Vollmer, S., 2017. Guidelines for sampling bedload transport with minimum uncertainty. Sedimentology 64, 1630–1645.

Gaeuman, D.A., Schmidt, J.C., Wilcock, P.R., 2003. Evaluation of in-channel gravel storage with morphology-based gravel budgets developed from planimetric data. Journal of Geophysical research 108 (F1), 6001.

Gilet, L., Gob., F., Gautier, E., Houbrechts, G., Virmoux, C., Thommeret, N., 2020. Hydro-morphometric parameters controlling travel distance of pebbles and cobbles in three gravel bed streams. Geomorphology 358, 107117.

Guillon, H., 2016. Origine et transport des sédiments dans un bassin versant alpin englacé (Glacier des Bossons, France) : une quantification couplant mesures hydro-sédimentaires haute-résolution,

929 suivi radio-fréquence de galets, teneur en nucléides cosmogéniques et méthodes probabilistes. Ph.
930 Thesis, Grenoble Alpes University.
931 Haschenburger, J.K., 2011a. The rate of fluvial gravel dispersion. Geophysical Research Letters 38,
932 L24403.
933 Haschenburger, J.K., 2011b. Vertical mixing of gravel over a long flood series. Earth Surface Processes
934 and Landforms 36, 1044-1058.
935 Haschenbuger, J.K., 2013a. Tracing river gravels: Insights into dispersion from a long-term field
936 experiment. Geomorphology 200, 121-131.
937 Haschenbuger, J.K., 2017. Streambed Disturbance over a Long Flood Series. River Research and
938 ApplicationsVolume 33 (5), 753-765.
939 Haschenburger, J.K., Wilcock, P.R., 2003. Partial transport in a natural gravel bed channel. Water
940 Resources Research 39, 1020.
941 Hassan, M.A., Bradley, D.N., 2017. Geomorphic controls on tracer particle dispersion in gravel bed
942 rivers. In: Tsutsumi, D., Laronne, J.B. (Eds.), Gravel-Bed Rivers, Processes and Disasters. Wiley-
943 Blackwell, UK, pp. 439-466.
944 Hassan, M.A., Church, M., 1992. The movement of individual grains on the streambed. In: Bili P, Hey,
945 R.D., Thorne, C.R., Tacconi, P. (Eds.), Gravel-bed rivers III: Dynamics of gravel-bed rivers. John
946 Wiley & Sons, Chichester, UK. pp. 159-175.
947 Hassan, M.A., Church, M., 2001. Sensitivity of bed load transport in Harris Creek : seasonal and spatial
948 variation over a cobble-gravel bar. Water Resources Research 37 (3), 813-825.
949 Hassan, M.A., Church, M., Schick, A.P., 1991. Distance of movement of coarse particles in gravel bed
950 streams. Water Resources Research 27 (4), 503-511.
951 Hassan, M.A., Saletti, M., Johnson, J.P.L., Ferrer-Boix, C., Venditti, J.G., Church, M., 2020.
952 Experimental insights into the threshold of motion in alluvial channels: Sediment supply and
953 streambed state. Journal of Geophysical Research: Earth Surface 125, e2020JF005736.
954 Hassan, M.A., Voepel, H., Schumer, R., Parker, G., Fraccarollo L., 2013. Displacement characteristics
955 of coarse fluvial bed sediment. Journal of Geophysical Research Earth Surface, 118 (1), 155-165.

Hassan, M.A., Woodsmith, R.D., 2004. Bed load transport in an obstruction-formed pool in a forest, gravelbed stream. Geomorphology 58, 203-221.

Haynes, H., Pender, G., 2007. Stress history effects on graded bed stability. Journal of Hydraulic Engineering 133 (4), 343-349.

Hill, B., 1975. A simple general approach to inference about the tail of a distribution. The Annals of Statistics 3 (5), 1163–1174.

Hodge, R.A., Sear, D.A., Leyland, J., 2013. Spatial variations in surface sediment structure in riffle–pool sequences: A preliminary test of the Differential Sediment Entrainment Hypothesis (DSEH). Earth Surface Processes and Landforms 38 (5), 449-465.

Houbrechts, H., Levecq, Y., Peeters, A., Hallot, E., Van Campenhout, J., Denis, A.C., Petit, F., 2015. Evaluation of long-term bedload virtual velocity in gravel-bed rivers (Ardenne, Belgium). Geomorphology 251, 6-19.

Houbrechts, G., Levecq, Y., Petit, F., 2012. Characterisation of sand transport in gravel-bed rivers using iron slag dated by historical studies. 2012 EGU General Assembly 2012, Vol. 14, EGU2012-4546.

Houbrechts, G., Levecq, Y., Vanderheyden, V., Petit, F., 2011. Long-term bedload mobility in gravel-bed rivers using iron slag as a tracer. Geomorphology 126, 233-244.

Iwasaki, T., Yamaguchi, S., Yabe, H., 2018. Numerical simulation of bedload tracer transport associated with sand bar formation, bank erosion, and channel migration. River Flow 2018 - Ninth International Conference on Fluvial Hydraulics E3S Web of Conferences 40, 02013.

Jackson, W.L., Beschta, R.L., 1984. Influences of Increased Sand Delivery on the Morphology of Sand and Gravel Channels1. JAWRA Journal of the American Water Resources Association 20, 527–533.

Kasprak, A., Wheaton, J.M., Ashmore, P.E., Hensleigh, J.W., Peirce, S., 2015. The relationship between particle travel distance and channel morphology: Results from physical models of braided rivers. Journal of Geophysical Research: Earth Surface 120, 55-74.

Keller, E.A., 1971. Areal sorting of bed-load material: The hypothesis of velocity reversal. Geological Society of America Bulletin 82, 753-756.

983 Keller, E.A., Florsheim, J.L., 1993. Velocity-reversal hypothesis: A model approach. Earth Surface
984 Processes and Landforms 18,733-740.
985 Knighton, D., 1998. Fluvial forms and processes, a new perspective. Arnold, London, UK, 383 p.
986 Kochel, R.C., 1988. Geomorphic impact of large floods: review and new perspectives on magnitude and
987 frequency. In: Baker, V.R., Kochel, R.C., Patton, P.C. (Eds.), Flood Geomorphology. Wiley &
988 Sons, New York, pp. 169-187.
989 Kondolf, G.M., Mathews, W.V.G., 1986. Transport of tracer gravels on a coastal California river.
990 Journal of Hydrology 85, 265-280.
991 Konrad, C.P., Booth, D.B., Burges, S.J., Montgomery, D.R., 2002. Partial entrainment of gravel bars
992 during floods. Water Resources Research 38 (7), 1104.
993 Lajeunesse, E., Devauchelle, O., Houssais, M., Seizilles G., 2013. Tracer dispersion in bedload
994 transport. Advances Geosciences 37, 1–6.
995 Lajeunesse, E., Devauchelle, O., James, F., 2018. Advection and dispersion of bed load tracers. Earth
996 Surface Dynamics 6, 389–399.
997 Lamarre, H., Roy, A.G., 2008. The role of morphology on the displacement of particles in a step–pool
998 river system. Geomorphology 99, 270-279.
999 Lane, S.N., Richards, K.S., Chandler, J.H., 1995. Morphological estimation of the time-integrated bed
1000 load transport rate. Water Resources Research 31 (3), 761-772.
1001 Larue, J. P., 1981. Les nappes alluviales de la vallée du Cher dans le bassin de Montluçon. Norois 111,
1002 345–360.
1003 Larue, J. P., 2011. Longitudinal profiles and knickzones: the example of the rivers of the Cher basin in
1004 the northern French Massif Central. Proceedings of the Geologists' Association 122, 125–142.
1005 Leopold, L.B., 1992. Sediment size that determines channel morphology. In: Bili, P., Hey, R.D., Thorne,
1006 C.R., Tacconi, P. (Eds.), Gravel-bed rivers III: Dynamics of gravel-bed rivers. John Wiley & Sons,
1007 Chichester, UK, pp. 297-311.
1008 Lewin, J., 1989. Floods in fluvial geomorphology. In: Beven, K., Carling, P. (Eds.), Floods:
1009 Hydrological, Sedimentological and Geomorphological Implications. Wiley & Sons, Chichester,
1010 pp. 265-284.

1011 Lisle, T.E., 1979. A sorting mechanism for a riffle-pool sequence: Summary. Geological Society of
1012 America Bulletin 90, 616-617.
1013 Lisle, T.E., Hilton, S., 1992. The volume of fine sediment in pools: An index of sediments supply in
1014 gravel-beds streams. JAWRA Journal of the American Water Resources Association 28 (2), 371-
1015 383.
1016 Lisle, T.E., Hilton, S., 1999. Fine bed material in pools of natural gravel bed channels. Water Resources
1017 Research 35 (4), 1291-1304.
1018 Lisle, T.E., Iseya, F., Ikeda, H., 1993. Response of a channel with alternate bars to a decrease in supply
1019 of mixed-size bed load: a flume experiment. Water Resources Research 29 (11), 3623-3629.
1020 Lisle, T.E., Nelson, J.M., Pitlick, J., Madej, M.A., Barkett, B.L., 2000. Variability of bed mobility in
1021 natural , gravel-bed channels and adjustments to sediment load at local and reach scales model to
1022 examine relations between local boundary shear stress channels with widely differing annual
1023 sediment values channels. Water Resources Research 36 (12), 3743-3755.
1024 MacVicar, B.J., Roy, A.G., 2007a. Hydrodynamics of a forced riffle pool in a gravel bed river: 1. Mean
1025 velocity and turbulence intensity. Water Resources Research 43, W12401.
1026 MacVicar, B.J., Roy, A.G., 2007b. Hydrodynamics of a forced riffle pool in a gravel bed river: 2. Scale
1027 and structure of coherent turbulent events. Water Resources Research 43, W12402.
1028 MacVicar, B.J., Roy, A.G., 2011. Sediment mobility in a forced riffle-pool. Geomorphology 125, 445-
1029 456.
1030 MacWilliams, Jr. M.L., Wheaton, J.M., Pasternack, G.B., Street, R.L., Kitanidis, P.K., 2006. Flow
1031 convergence routing hypothesis for pool-riffle maintenance in alluvial rivers. Water Resources
1032 Research 42, W10427.
1033 Magilligan, F.J., 1992. Thresholds and the spatial variability of flood power during extreme floods.
1034 Geomorphology 5, 373-390.
1035 Mao, L., 2012. The effect of hydrographs on bed load transport and bed sediment spatial arrangement.
1036 Journal of Geophysical Research 117, F03024.

1037 Masteller, C.C., Finnegan, N.J.,Turowski, J.M., Yager, E.M., &Rickenmann, D., 2019.
1038 History-dependent threshold for motion revealed by continuous bedload transport measurements
1039 in a steep mountain stream. Geophysical ResearchLetters 46, 2583–2591.
1040 May, C.L., Pryor, S., 2014. Initial motion and bedload transport distance determined by tracking in a
1041 large regulated river. River Research and Application 30 (4), 508-520.
1042 McDowell C., Hassan, M.A., 2020. The influence of channel morphology on bedload path lengths:
1043 Insights from a survival process model. Earth Surface Processes and Landforms 45 (12), 2982–
1044 2997.
1045 McDowell, C., Gaeuman, D., Hassan, M.A., 2021. Linkages between bedload displacements and
1046 topographic change. Earth Surface Processes and Landforms 46 (15), 3127-3142.
1047 McEwan, I.K., Habersack, H.M., Heald, J.G.C., 2001. Discrete particle modelling and active tracers:
1048 New techniques for studying sediment transport as Lagrangian phenomenon. In: Gravel Bed
1049 Rivers V., Mosley, P. (Eds). New Zealand Hydrological Society: Wellington, NZ, pp. 339-360.
1050 McQueen, R., Ashmore, P., Millard, T., Goeller, N., 2021. Bed particle displacements and
1051 morphological development in a wandering gravelbed river. Water Resources Research, 57,
1052 e2020WR027850.
1053 Milan, D.J., 2013. Sediment routing hypothesis for pool-riffle maintenance. Earth Surface Processes
1054 and Landforms 38 (14), 1623-1641.
1055 Milan, D.J., Heritage, G.L., Large, A.R.G., 2002. Tracer pebble entrainment and deposition loci:
1056 Influence of flow character and implications for riffle–pool maintenance. In: Jones, S.J., Frostick,
1057 L.E. (Eds.), Sediment flux to basins: Causes, controls and consequences. Geological Society of
1058 London Special Publications 191, pp. 133-148.
1059 Milan, D.J., Heritage, G.L., Large, A.R.G., Charlton, M.E., 2001. Stage dependent variability in tractive
1060 force distribution through a riffle–pool sequence. Catena 44, 85-109.
1061 Monteith, H., Pender, G., 2005. Flume investigations into the influence of shear stress history on a
1062 graded sediment bed. Water Resources Research 41, W12401.
1063 Neill, C.R., 1971. River bed transport related to meander migration rates. Journal of the Waterways,
1064 Harbors, and Coastal Engineering Division, ASCE 97, 783-786.

1065 Neill, C.R., 1987. Sediment balance considerations linking long-term transport and channel processes.
1066 In: Thorne, C.R., Bathurst, J.C., Hey, R.D. (Eds.), Gravel-bed rivers III: Sediment transport in
1067 gravel-bed rivers. John Wiley & Sons, Chichester, UK, pp. 225-240.
1068 Nelson, P.A., Venditti, J.G., Dietrich, W.E., Kirchner, J.W., Ikeda, H., Iseya, F., Sklar, L.S., 2009.
1069 Response of bed surface patchiness to reductions in sediment supply. Journal of Geophysical
1070 Research 114, F02005.
1071 Ockelford, A.M., Haynes, H., 2013. The impact of stress history on bed structure. Earth Surface
1072 Processes and Landforms 38 (7), 717-727.
1073 Paintal, A.S., 1971. A stochastic model of bed load transport. Journal of Hydraulic Research 9 (4): 527-
1074 554.
1075 Papangelakis, E., Hassan M.A., 2016. The role of channel morphology on the mobility and dispersion
1076 of bed sediment in a small gravel-bed stream. Earth Surface Processes and Landforms 41 (15),
1077 2191-2206.
1078 Paphitis, D., Collins, M.B., 2005. Sand grain threshold, in relation to bed "stress history": an
1079 experimental study. Sedimentology 52, 827-838.
1080 Parker, G., Klingeman, P.C., McLean, D.L., 1982. Bedload and size distribution in paved gravel-bed
1081 streams. Journal of Hydraulic Engineering 108, 544-571.
1082 Pelosi, A., Schumer, R., Parker, G., Ferguson, R.I., 2016. The cause of advective slowdown of tracer
1083 pebbles in rivers: Implementation of Exner-Based Master Equation for coevolving streamwise and
1084 vertical dispersion, Journal of Geophysical Research 121 (3), 623-637.
1085 Petit, F., 1987. The relationship between shear stress and the shaping of the bed of a pebble-loaded
1086 river, La Rulles – Ardenne. Catena 14, 453-468.
1087 Pierce, J.K., Hassan, M.A., 2020. Back to Einstein: Burial-induced three-range diffusion in fluvial
1088 sediment transport. Geophysical Research Letters 47, e2020GL087440.
1089 Pyrce, R.S., Ashmore, P.E., 2003a. Particle path length distributions in meandering gravel-bed streams:
1090 Results from physical models. Earth Surface Processes and Landforms 28, 951-966.
1091 Pyrce, R.S., Ashmore, P.E., 2003b. The relation between particle path length distributions and channel
1092 morphology in gravel-bed streams: A synthesis. Geomorphology 56, 167-187.

1093 Pyrce, R.S., Ashmore, P.E., 2005. Bedload path length and point bar development in gravel-bed river
1094 models. Sedimentology 52, 839-857.
1095 Recking, A., 2010. A comparison between flume and field bed load transport data and consequences for
1096 surface-based bed load transport prediction. Water Resources Research 46, W03518.
1097 Recking, A., Piton, G., Vázquez-Tarrío, D., Parker, A., 2016. Quantifying the Morphological Print of
1098 Bedload Transport. Earth Surface Processes and Landforms 41 (6), 809-822.
1099 Reid, I., Frostick, L.E., Layman, J.T., 1985. The incidence and nature of bedload transport during flood
1100 flows in coarse-grained alluvial channels. Earth Surface Processes and Landforms 10, 33-44.
1101 Reid, S.C., Lane, S.N., Berney, J.M., Holden, J., 2007. The timing and magnitude of coarse sediment
1102 transport events within an upland, temperate gravel-bed river. Geomorphology 83, 152-182.
1103 Rickenmann, D., Recking, A., 2011. Evaluation of flow resistance in gravel-bed rivers through a large
1104 field data set. Water Resources Research 47 (7), W07538.
1105 Roseberry, J.C., Schmeeckle, M.W., Furbish, D.J., 2012. A probabilistic description of the bed load
1106 sediment flux: 2. Particle activity and motions. Journal of Geophysical Research 117, F03032.
1107 Schmidt, K.H., Gintz, D., 1995. Results of bedload tracer experiments in a mountain river. In: Hickin,
1108 E.J. (Eds.). River Geomorphology. John Wiley & Sons, Chichester, UK, pp. 37-54.
1109 Sear, D.A., 1996. Sediment transport process in pool-riffle sequences. Earth Surface Processes and
1110 Landforms 21, 241-262.
1111 Simon-Coinçon, R., Thiry, M., Quesnel, F., 2000. Paléopaysages et paléoenvironnements
1112 sidérolithiques du Nord du Massif central (France). Comptes Rendus de l′Académie des Sciences
1113 - Series IIA - Earth and Planetary Science 330, 693–700.
1114 Thompson D.M., 2007. The characteristics of turbulence in a shear zone downstream of a channel
1115 constriction in a coarse-grained forced pool. Geomorphology 83, 199–214.
1116 Thompson, D.M., 2011. The velocity-reversal hypothesis revisited. Progress in Physical Geography 35
1117 (1), 123-132.
1118 Thompson, D.M., MacVicar, B.J., 2020. Pool-Riffle. In: Reference Module in Earth Systems and
1119 Environmental Sciences, Elsevier.

1120 Thomspon, D.M., Whol, E.E., 2009. The linkage between velocity patterns and sediment entrainment
1121 in a forced-pool and riffle unit. Earth Surface Processes and Landforms 34, 177-192.
1122 Thompson, D.M., Wohl, E.E., Jarrett, R.D., 1999. Velocity reversals and sediment sorting in pools and
1123 riffles controlled by channel constrictions. Geomorphology 27, 229-241.
1124 Turland, M., Cojean, R., Brulhet, J., Morice, E., Grolier, J., Lacour, A., 1989a. Carte géol. France
1125 (1/50000), feuille Hérisson (596), BRGM, Orléans.
1126 Turland, M., Hottin, A.M., Cojean, R., Ducreux, J.L., Debéglia, N., d'Arcy, D., Mathis, V., Carroué,
1127 J.P., Piboule, M., 1989b. Notice explicative, Carte géol. France (1/50000), feuille Hérisson (596),
1128 BRGM, Orléans, 118 p.
1129 Vahidi, E., Rodríguez, J.F., Bayne, E., Saco, P.M., 2020. Oneflood is not enough: Pool‐riffle self-
1130 maintenance under time‐varying flows and non equilibrium multifractional sediment
1131 transport.Water ResourcesResearch 56, e2019WR026818.
1132 Vayssière, A., Castanet, C., Gautier, E., Virmoux, C., Dépret, T., Gandouin, E., Develle-Vicent A.L.,
1133 Mokadem, F., Saulnier-Copard, S., Sabatier, P., Carcaud, N., 2020. Long-term readjustments of a
1134 sinuous river during the second half of the Holocene in northwestern Europe (Cher River, France).
1135 Geomorphology 370, 107395.
1136 Vázquez-Tarrío, D., Batalla, R.J., 2019. Assessing Controls on the Displacement of Tracers in Gravel-
1137 Bed Rivers. Water 11 (8), 1598.
1138 Vázquez-Tarrío, D., Piqué, G., Vericat, D., Batalla, R.J., 2021. The active layer in gravel-bed rivers: An
1139 empirical appraisal. Earth Surface Processes and Landforms 46 (2), 323-343.
1140 Vázquez-Tarrío, D., Recking, A., Liébault, F., Tal, M., Menéndez-Duarte, R., 2019. Particle transport
1141 in gravel-bed rivers: Revisiting passive tracer data. Earth Surface Processes and Landforms 44 (1),
1142 112-128.
1143 Whiting, P.J., Stamm, J.F., Moog, D.B., Orndorff, R.L., 1999. Sediment-transporting flows in headwater
1144 streams. Geological Society of America Bulletin 111 (3), 450-466.
1145 Wilcock, P.R., 1998. Two-fraction model of initial sediment motion in gravel-bed rivers. Science 280
1146 (5362), 410-412.

1147 Wilcock, P.R., Crowe, J.C., 2003. Surface-based transport model for mixed-size sediment. Journal of
1148 Hydraulic Engineering 129 (2), 120-128.
1149 Wilcock, P.R., McArdell, B.W., 1993. Surface-based fractional transport rates: Mobilization thresholds
1150 and partial transport of a sand-gravel sediment. Water Resources Research 29 (4), 1297-1312.
1151 Wilkinson, S.N., Keller, R.J., Rutherfurd, I.D., 2004. Phase-shifts in shear stress as an explanation for
1152 the maintenance of pool-riffle sequences. Earth Surface Processes and Landforms 29, 737-753.
1153 Wolman, M.G., 1954. A method of sampling coarse river-bed material. Transactions of the American
1154 Geophysical Union 35 (6), 951-956.
1155 Wu, Z., Singh, A., Fu, X., Wang, G., 2019. Transient anomalous diffusion and advective slowdown of
1156 bedload tracers by particle burial and exhumation. Water Resources Research 55 7964–7982.
1157 Zhang, Y., Meerschaert, M.M., Packman, A.I., 2012. Linking fluvial bed sediment transport across
1158 scales. Geophysical Research Letters 39 (20), L20404.